Development of the southern Eastern Cordillera, NW Argentina, constrained by apatite fission track thermochronology: From early Cretaceous extension to middle Miocene shortening

Anke Deeken,[1,2] Edward R. Sobel,[2] Isabelle Coutand,[3] Michael Haschke,[4] Ulrich Riller,[5] and Manfred R. Strecker[2]

Received 23 August 2005; revised 4 July 2006; accepted 15 August 2006; published 18 November 2006.

[1] For the Puna Plateau and Eastern Cordillera of NW Argentina, the temporal and spatial pattern of deformation and surface uplift remain poorly constrained. Analysis of completely and partially reset apatite fission track samples collected from vertical profiles along an ESE trending transect extending from the plateau interior across the southern Eastern Cordillera at ~25°S reveals important constraints on the deformation and exhumation history of this part of the Andes. The data constrain the Neogene Andean development of the Eastern Cordillera as well as rift-related exhumation for some of the sampled locations in the Late Jurassic/Early Cretaceous. An intervening Eocene-Oligocene exhumation episode in the southern Eastern Cordillera was probably related to crustal shortening. Subsequent reburial of the area by Andean foreland basin strata commenced between 30 and 25 Myr. Magnitude and duration of sedimentation, revealed by thermal modeling, differ between the sample locations, pointing to an eastward propagating basin system. In the southern Eastern Cordillera, Andean deformation commenced at 22.5–21 Myr, predating both the inferred formation of significant topography by 5–7.5 Myr and preservation of sediments in the adjacent Cenozoic basins by 6.5–8 Myr. Comparing the calculated structural depth of partially reset samples suggests that newly formed west dipping reverse faults along the former Salta Rift margin accommodated most of the Neogene tectonic movement. Late Cenozoic deformation at the southern Eastern Cordillera began earlier in the west and subsequently propagated eastward. The lateral growth of the orogen is coupled with a foreland basin system developing in front of the range and then becomes subsequently compartmentalized by later emergent topography. **Citation:** Deeken, A., E. R. Sobel, I. Coutand, M. Haschke, U. Riller, and M. R. Strecker (2006), Development of the southern Eastern Cordillera, NW Argentina, constrained by apatite fission track thermochronology: From early Cretaceous extension to middle Miocene shortening, *Tectonics*, *25*, TC6003, doi:10.1029/2005TC001894.

1. Introduction

[2] Knowledge of the temporal and spatial pattern of deformation and surface uplift are prerequisites for understanding the development of orogenic systems. Often, sedimentologic and provenance data are used to infer orogenic growth. However, a complementary method of unraveling the complex history of mountain belts is using apatite fission track (AFT) thermochronology along vertical profiles through an uplifted section of crust to obtain information on the onset and the rate of rock exhumation.

[3] The timing of orogen-normal shortening on the present-day Puna Plateau and in the Eastern Cordillera of northwestern Argentina (Figure 1a) that led to formation of the modern Andes remains controversial. The main phase of Andean deformation in the southern central Andes was thought to have started between 20 and 15 Myr [e.g., *Jordan and Alonso*, 1987; *Allmendinger et al.*, 1997; *Jordan et al.*, 1997], while recent investigations suggest that tectonic movements already occurred in late Eocene-Oligocene time [*Kraemer et al.*, 1999; *Adelmann*, 2001; *Coutand et al.*, 2001; *Carrapa et al.*, 2005; *Coutand et al.*, 2006]. AFT data from the eastern margin of the Puna and from within the southern Eastern Cordillera document rapid exhumation in Sierra de Chango Real between 38 ± 3 and 29 ± 3 Myr [*Coutand et al.*, 2001] and Sierra Santa Rosa de Tastil at 30 ± 3 Myr, respectively [*Andriessen and Reutter*, 1994] (Figure 1a); comparable FT cooling ages were determined for detrital apatites from the Angastaco basin [*Coutand et al.*, 2006]. Similarly, *Carrapa et al.* [2005] document rapid exhumation during the late Oligocene linked with tectonic range uplift in the interior of the present-day Puna, which was coupled with the formation of internally drained basins. Most investigations on the uplift and deformation of this region are based on the sedimentary record of basins adjacent to the uplifting ranges [e.g., *Jordan*, 1984; *Jordan and Alonso*, 1987; *Allmendinger et al.*, 1997; *Grier and*

[1]Institut für Geowissenschaften, Freie Universität Berlin, Berlin, Germany.
[2]Institut für Geowissenschaften, Universität Potsdam, Potsdam, Germany.
[3]UMR-CNRS 8110, UFR des Sciences de la Terre, Université des Sciences et Technologies de Lille 1, Villeneuve d'Ascq, France.
[4]School of Earth, Ocean and Planetary Sciences, Cardiff University, Cardiff, UK.
[5]Museum, Humboldt Universität Berlin, Berlin, Germany.

0278-7407/06/2005TC001894

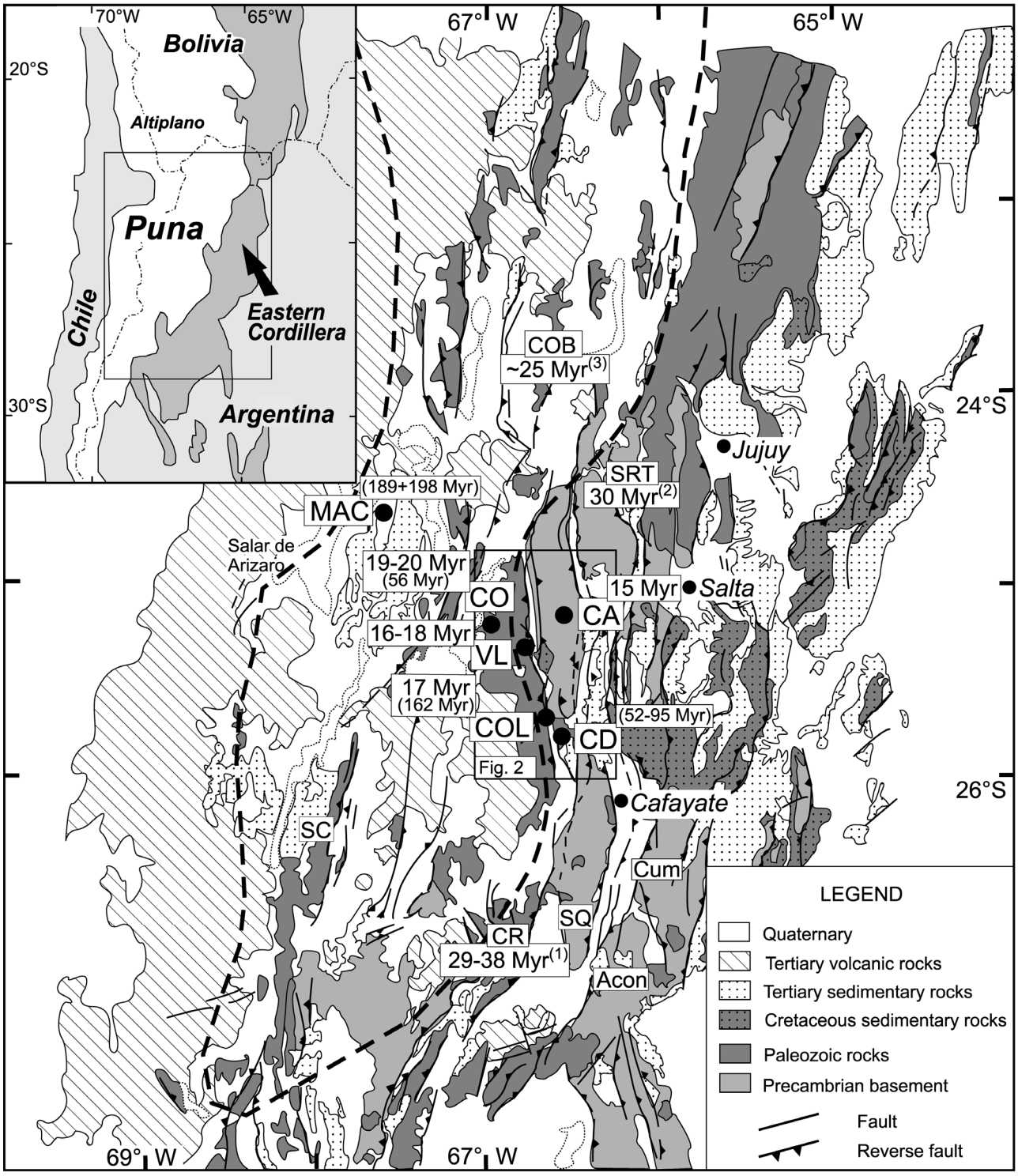

Figure 1a. Simplified geological map of the southern central Andes, NW Argentina (modified from *Mon and Salfity* [1995] (AAPG©, reprinted by permission of the AAPG whose permission is required for further use), and location of study area. The dashed line delineates the Puna Plateau. Black circles indicate sample locations with apparent AFT ages in Myr (ages of partially reset samples in parentheses): CA, Cachi; CD, Cerro Durazno; CO, Complejo Oire; COL, Colome; MAC, Sierra de Macon; VL, Valle Luracatao. Further abbreviations are as follows: Acon, Sierra Aconquija; COB, Cobres Granite; CR, Chango Real; Cum, Cumbres Calchaquíes; SC, Sierra Calalaste; SQ, Sierra Quilmes; SRT, Sierra Santa Rosa de Tastil. Cited AFT ages are from (1) *Coutand et al.* [2001], (2) *Andriessen and Reutter* [1994], and (3) *Deeken et al.* [2005].

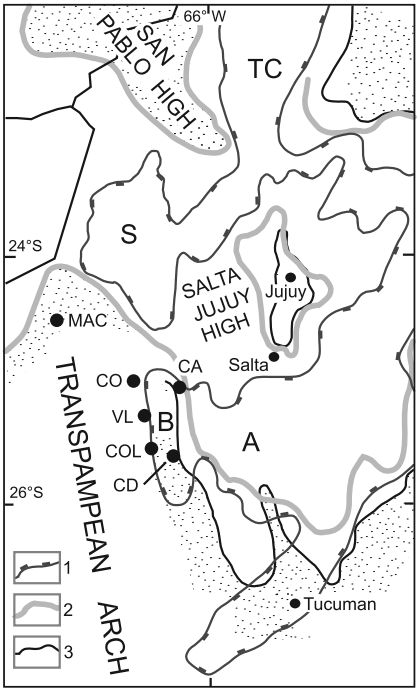

Figure 1b. Map of the Salta Rift showing part of the main structural highs and subbasins during the synrift and postrift stages (modified from *Marquillas et al.* [2005] with permission from Springer). Key is as follows: 1, synrift stage basin margin; 2, early postrift stage basin margin; 3, late postrift stage basin margin. Dotted area represents topographic highs during this stage. Subbasins are A, Alemanía; B, Brealito; S, Sey; TC, Tres Cruces. The black circles indicate sample locations (for abbreviations, see Figure 1a).

Dallmeyer, 1990]. However, the basins within the Puna and along its eastern margin are spatially discontinuous and diachronous [*Strecker et al.*, 1989; *Allmendinger et al.*, 1997; *Sobel et al.*, 2003; *Hilley and Strecker*, 2004], and the paucity of radiometrically dated volcanic ashes and gaps in biostratigraphy in these basin sediments have precluded the precise determination of the timing of deformation. In addition, in settings where young strata overlie resistant basement, the appearance of coarse clastic material in the basin can substantially postdate the onset of exhumation [e.g., *Sobel and Strecker*, 2003].

[4] Extensional structures of the Cretaceous/Paleogene Salta Rift have strongly influenced Tertiary Andean deformation styles in the Eastern Cordillera; the orientation of specific structures with respect to the trend of Andean shortening appears to have exerted a first-order control on reactivation of these structures [*Bianucci et al.*, 1982; *Grier et al.*, 1991; *Mon and Salfity*, 1995; *Cristallini et al.*, 1997; *Kley et al.*, 1999, 2005; *Mortimer et al.*, 2006]. For example, at the southern terminus of the Eastern Cordillera at ~25°S, where the range markedly broadens [*Grier et al.*, 1991], the distinct boundary of the plateau has a pronounced westward recess (Figure 1a). Here, the plateau margin is formed by several basement uplifts with elevations exceeding 5500 m that mark the transition from the southern Eastern Cordillera to the Sierras Pampeanas farther south. These ranges divide the high plateau to the west and north from the lower elevation parts of the southern Eastern Cordillera to the southeast [*Grier et al.*, 1991]. This sector of the Eastern Cordillera developed within the Brealito and Alemanía subbasins of the former Salta Rift [*Grier et al.*, 1991] (Figure 1b), and the ranges that were uplifted during the Cenozoic have been inferred to represent the former rift margin [*Hongn and Seggiaro*, 2001]. Within the former Brealito subbasin, the basal synrift deposits are presently exposed at different elevations, suggesting that faults were reactivated to various degrees during Andean crustal shortening and basin inversion [*Hongn and Seggiaro*, 2001]. This arrangement of faults and strata thus provides an ideal setting to examine the influence of rift structures on the locus of Cenozoic deformation.

[5] In order to decipher the spatial and temporal development of deformation and surface uplift in this region, samples from six locations were collected for AFT thermochronology. Sampling focused on the basement ranges along the eastern margin of the Puna Plateau, complementary samples come from the Salar de Arizaro basin on the plateau, and from ranges within the southern sectors of the Eastern Cordillera (Figures 1a, 1b, 2, and 3). Most of the sampling transects extend across significant relief and yielded abundant track length data, allowing the results to be interpreted in terms of variable exhumation rates through time.

[6] The study area has a complex Mesozoic/Cenozoic history, characterized by rift-related exhumation, burial beneath Cenozoic sedimentary basin strata, and renewed exhumation of the formerly buried basement ranges. Thermal modeling is therefore required in order to quantify the magnitude of this burial reheating. The consequences of this reburial for landscape evolution models are also important, as rock erodibility changes in the course of the exhumation history: while the youngest soft sediments are removed, increasingly more resistant bedrock is ultimately exposed. As the balance between exhumation and surface uplift is strongly influenced by variations in rock erodibility, combining stratigraphic and structural data with thermal modeling results also yields valuable insights into the topographic evolution of the world's second largest plateau and its adjacent regions.

2. Regional Geologic Setting

[7] On the Argentine Puna Plateau and within the Eastern Cordillera, numerous, partly isolated contractional basins are separated by meridional-trending ranges (Figure 1a). In addition, several Miocene-Pliocene volcanic chains cross the plateau along NW-SE striking fault systems [e.g., *Allmendinger et al.*, 1983; *Alonso et al.*, 1984; *Allmendinger et al.*, 1997; *Riller et al.*, 2001]. The ranges that reach elevations in excess of 5000 m, are bounded either by high-angle reverse faults or thrusts on one or

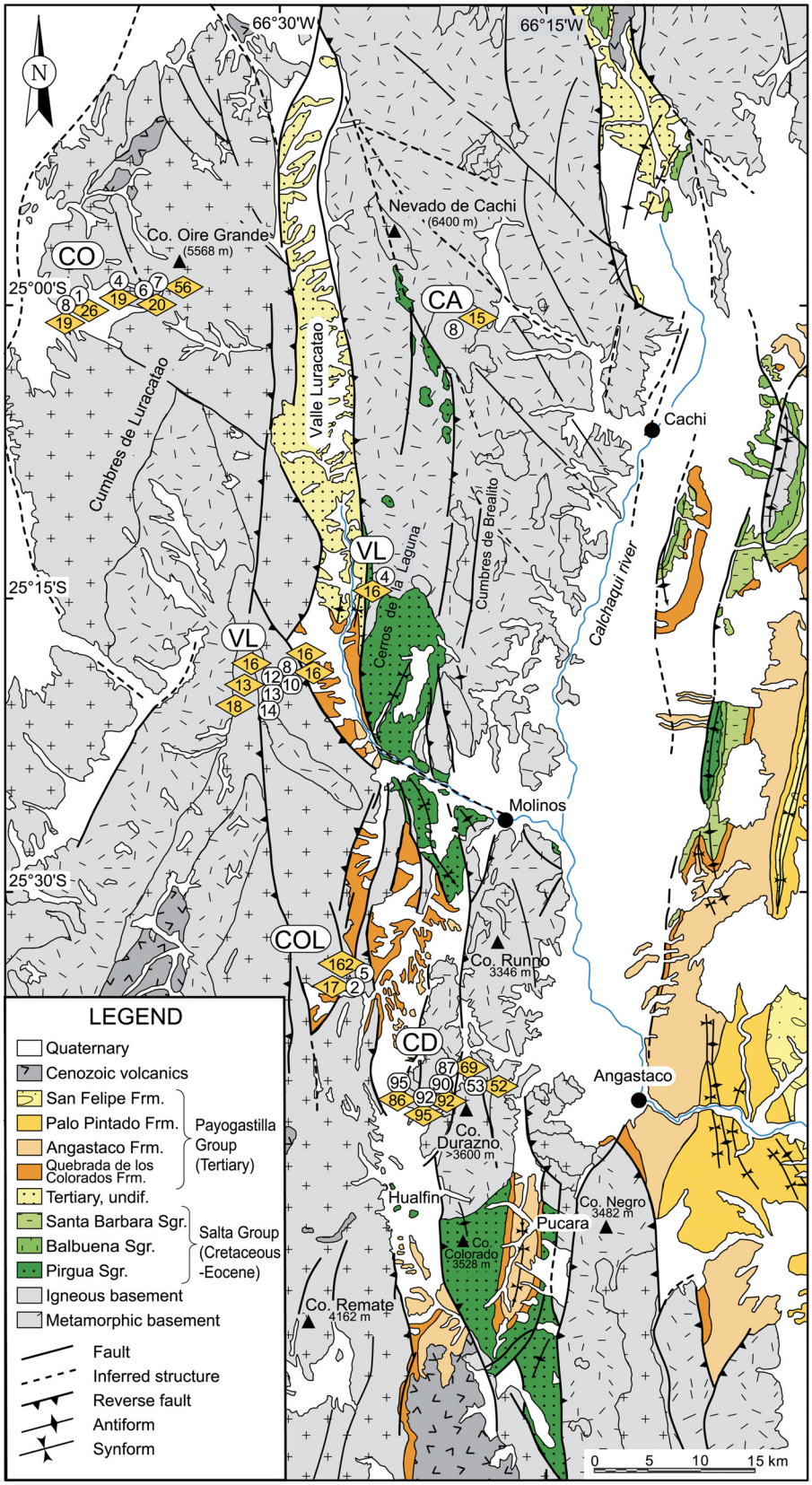

Figure 2. Geological map of the study area (modified from *Hongn and Seggiaro* [2001] and *Blasco et al.* [1996]). The white circles indicate sample numbers; the yellow rhombs indicate apparent AFT ages in Myr (for abbreviations, see Figure 1a).

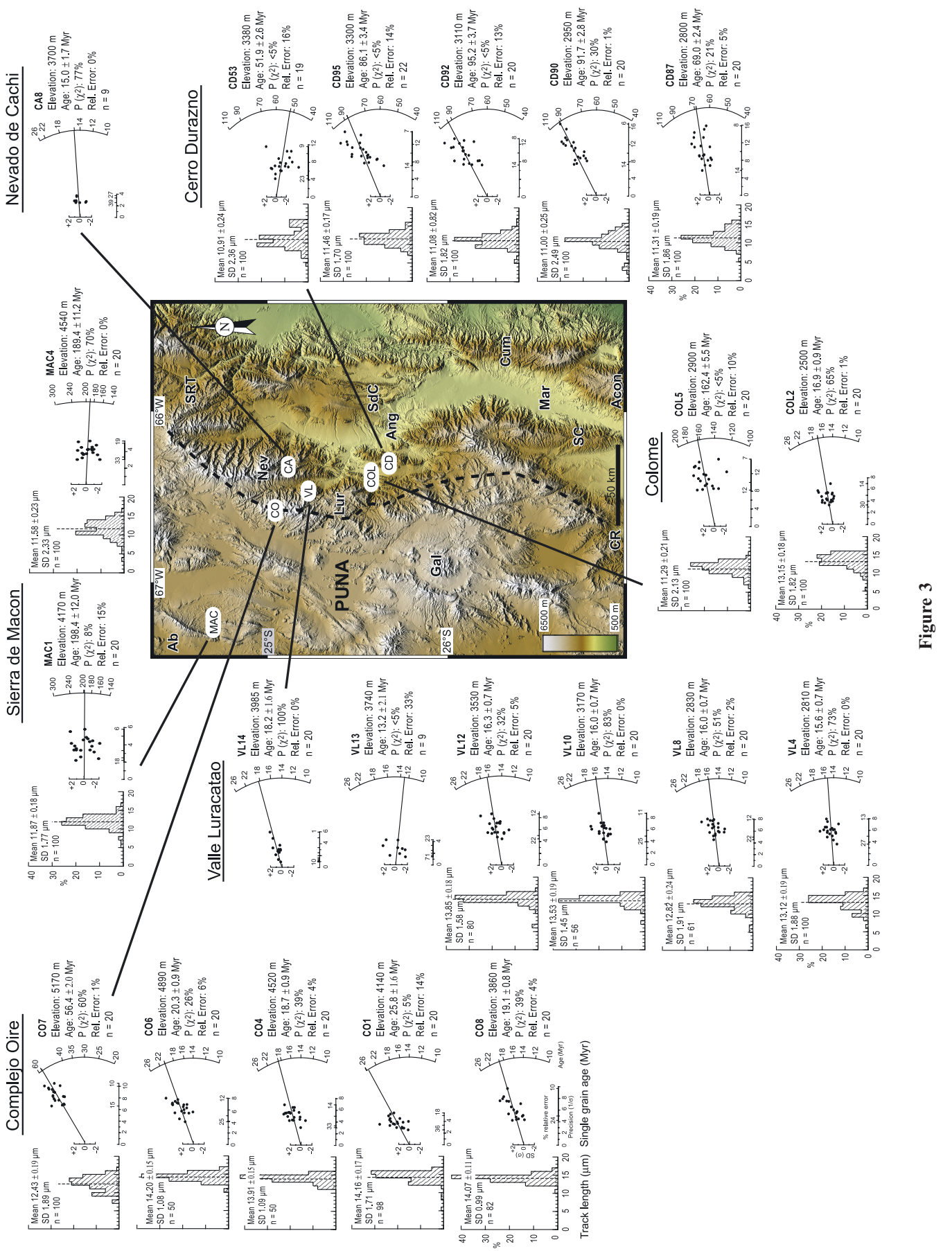
Complejo Oire
Sierra de Macon
Valle Luracatao
Cerro Durazno
Nevado de Cachi
Colome
PUNA
Ab
MAC
SRT
Nev
CA
CO
VL
Lur
COL
CD
SdC
Ang
Gal
Cum
Mar
SC
Acon
CR
67°W
66°W
25°S
26°S
N
50 km
6500 m
500 m
CO7 Elevation: 5170 m Age: 56.4 ± 2.0 Myr P (χ²): 60% Rel. Error: 1% n = 20
CO6 Elevation: 4890 m Age: 20.3 ± 0.9 Myr P (χ²): 26% Rel. Error: 6% n = 20
CO4 Elevation: 4520 m Age: 18.7 ± 0.9 Myr P (χ²): 39% Rel. Error: 4% n = 20
CO1 Elevation: 4140 m Age: 25.8 ± 1.6 Myr P (χ²): 5% Rel. Error: 14% n = 20
CO8 Elevation: 3860 m Age: 19.1 ± 0.8 Myr P (χ²): 39% Rel. Error: 4% n = 20
MAC1 Elevation: 4170 m Age: 198.4 ± 12.0 Myr P (χ²): 8% Rel. Error: 15% n = 20
MAC4 Elevation: 4540 m Age: 189.4 ± 11.2 Myr P (χ²): 70% Rel. Error: 0% n = 20
VL14 Elevation: 3985 m Age: 18.2 ± 1.6 Myr P (χ²): 100% Rel. Error: 0% n = 20
VL13 Elevation: 3740 m Age: 13.2 ± 2.1 Myr P (χ²): <5% Rel. Error: 33% n = 9
VL12 Elevation: 3530 m Age: 16.3 ± 0.7 Myr P (χ²): 32% Rel. Error: 5% n = 20
VL10 Elevation: 3170 m Age: 16.0 ± 0.7 Myr P (χ²): 83% Rel. Error: 0% n = 20
VL8 Elevation: 2830 m Age: 16.0 ± 0.7 Myr P (χ²): 51% Rel. Error: 2% n = 20
VL4 Elevation: 2810 m Age: 15.6 ± 0.7 Myr P (χ²): 73% Rel. Error: 0% n = 20
CD53 Elevation: 3380 m Age: 51.9 ± 2.6 Myr P (χ²): <5% Rel. Error: 16% n = 19
CD95 Elevation: 3300 m Age: 86.1 ± 3.4 Myr P (χ²): <5% Rel. Error: 14% n = 22
CD92 Elevation: 3110 m Age: 95.2 ± 3.7 Myr P (χ²): <5% Rel. Error: 13% n = 20
CD90 Elevation: 2950 m Age: 91.7 ± 2.8 Myr P (χ²): 30% Rel. Error: 1% n = 20
CD87 Elevation: 2800 m Age: 69.0 ± 2.4 Myr P (χ²): 21% Rel. Error: 5% n = 20
COL5 Elevation: 2900 m Age: 162.4 ± 5.5 Myr P (χ²): <5% Rel. Error: 10% n = 20
COL2 Elevation: 2500 m Age: 16.9 ± 0.9 Myr P (χ²): 65% Rel. Error: 1% n = 20
CA8 Elevation: 3700 m Age: 15.0 ± 1.7 Myr P (χ²): 77% Rel. Error: 0% n = 9
Track length (μm)
Single grain age (Myr)

Figure 3

both sides. They often consist of metamorphic and granitic basement (Figure 2), which records a complex Proterozoic to early Paleozoic history [e.g., *Mon and Salfity*, 1995; *Allmendinger et al.*, 1997] and later Mesozoic and Cenozoic overprint [*Mon and Salfity*, 1995].

[8] The continental Salta Rift developed in late Jurassic to early Cretaceous time (Figure 1b) [*Salfity*, 1982; *Galliski and Viramonte*, 1988; *Salfity and Marquillas*, 1994]; effusion of the rift-related Alto de Las Salinas basalts and rhyolites at 128–112 Myr (K/Ar, whole rock) [*Bossi*, 1969; *Bossi and Wampler*, 1969] marks the onset of synrift sedimentation in the southernmost part of the rift basin. The rift basin contains the Salta Group, comprising the synrift Kimmeridgian(?)-Campanian Pirgua Subgroup, and the Campanian to middle Eocene postrift Balbuena and Santa Barbara Subgroups [*Marquillas and Salfity*, 1988; *Salfity and Marquillas*, 1994; *Mon and Salfity*, 1995]. The Pirgua Subgroup rests unconformably on basement rocks [*Marquillas et al.*, 2005]. In the Brealito subbasin, the present-day Luracatao and Hualfin/Pucará valleys (Figures 1b and 2), syntectonic coarse conglomerates with thicknesses surpassing 4000 m adjacent to basin-bounding normal faults document considerable subsidence [*Marquillas et al.*, 2005]. The north striking reverse faults bounding the eastern flank of Cumbres de Luracatao (Figure 2) were most likely the principal structures defining the former rift margin [*Hongn and Seggiaro*, 2001]. The upper Pirgua Subgroup in the Brealito subbasin is largely eroded and postrift strata are absent, which likely reflects basin inversion during the late Eocene to early Oligocene [*Boso et al.*, 1984; *Marquillas et al.*, 2005]. Furthermore, Pirgua sedimentary rocks are thrust on Tertiary strata west of the Cerros de la Laguna and the Cerro Colorado (Figure 2) [*Hongn and Seggiaro*, 2001]. The postrift Balbuena and Santa Barbara Subgroups (Figure 2) reach a combined thickness of up to 1900 m in former depocenters east of Angastaco [*Marquillas et al.*, 2005]. An intercalated shallow marine sequence (Yacoraite Formation) in the Balbuena Subgroup indicates a shallow epicontinental sea in the Maastrichtian [*Salfity*, 1980, 1982; *Salfity and Marquillas*, 1994].

[9] The basement and the sedimentary rocks of the former Salta Rift basin are unconformably overlain by Cenozoic foreland basin strata. In the Angastaco area they are represented by the Payogastilla Group (Figure 2) [e.g., *Díaz and Malizzia*, 1983]. The basal, 340–600 m thick Quebrada de los Colorados Formation [*Hongn and Seggiaro*, 2001] consists of coarse-grained sandstones (sometimes conglomeratic) that grade upward into fine- to medium-grained sandstones and siltstones with paleosols [*Díaz et al.*, 1987; *Grier*, 1990]. Its poorly constrained age was attributed either to the early Miocene [*Díaz et al.*, 1987; *Grier*, 1990], to the Oligocene [*Starck and Vergani*, 1996] or even to the late Eocene [*Russo and Serraiotto*, 1978; *Díaz and Malizzia*, 1983]. These units are overlain by sandstones, siltstones, and conglomerates, deposited in a foreland setting, beginning at 14.5 Myr to about 2 Myr (Angastaco, Palo Pintado, and San Felipe formations) [e.g., *Díaz and Malizzia*, 1983; *Díaz et al.*, 1987; *Díaz and Miserendino Fuentes*, 1988; *Grier and Dallmeyer*, 1990; *Starck and Vergani*, 1996; *Coutand et al.*, 2006; G. Vergani and D. Starck, Geología del Sur de la Provincia de Salta-parte II: Estratigrafía y evolución tectosedimentaria del Cenozoico entre el Valle Calchaquí y Metán, Y.P.F. unpublished report, 1989, hereinafter referred to as Vergani and Starck, unpublished report, 1989]. Together, the units of the Payogastilla Group attain a thickness of 6000 m and were faulted and folded before about 2 Myr (M. R. Strecker, unpublished data, 2005). Climatic indicators throughout the lower part of the stratigraphic section point to dominantly arid climate conditions [*Starck and Anzótegui*, 2001], which were superseded by humid conditions between ~9 and ~5 Myr, whereas late Pliocene units indicate a return to arid conditions [*Starck and Vergani*, 1996; *Starck and Anzótegui*, 2001; *Coutand et al.*, 2006; Vergani and Starck, unpublished report, 1989].

[10] In contrast, climate remained arid in the intramontane basins within the present Puna to the west [*Alonso et al.*, 1991; *Alonso*, 1992; *Vandervoort et al.*, 1995, *Alonso et al.*, 2006]. From the occurrence of thick evaporites, *Vandervoort et al.* [1995] deduced the existence of internal drainage on the southern Puna and hence uplift of the eastern plateau margin by no later than 15 Myr that acted as an orographic barrier to moisture-bearing easterly winds. On the basis of provenance studies, *Coutand et al.* [2006] suggested that a drainage divide already existed to the north and northwest of the Angastaco basin by middle Miocene time. Limited published paleocurrent data indicate that sediments deposited in the Angastaco basin were derived from western to northwestern sources [*Salfity et al.*, 1984; *Díaz and Miserendino Fuentes*, 1988; *Starck and Anzótegui*, 2001; *Coutand et al.*, 2006]. In the Pliocene, a shift to westward transport directions occurred, accompanied by a change in provenance and increasing aridification in the Angastaco basin, suggesting that at that time a new orographic barrier, the Sierra de los Colorados, was uplifted east of the Angastaco basin [*Starck and Anzótegui*, 2001; *Coutand et al.*, 2006]. The successive eastward building of

Figure 3. Radial plots and track length histograms for all vertical transects. Sample locations are indicated by white circles in the DEM of the southern central Andes. Data are from the SRTM 90 m square grid DEM. The dashed line demarcates the boundary between the internally drained Puna Plateau and the foreland that drains to the east. For all samples that passed the χ^2 test, the pooled age is reported; for samples with $P(\chi^2) < 5\%$ the central age is used. Error is $\pm 1\sigma$. For abbreviations of sample locations, see Figure 1a; further abbreviations are as follows: Ab, Arizaro basin; Acon, Sierra Aconquija; Ang, Angastaco basin; CR, Sierra de Chango Real; Cum, Cumbres Calchaquíes; Gal, Cerro Galán; Lur, Cumbres de Luracatao; Mar, Santa María basin; Nev, Nevado de Cachi; SC, Sierra Quilmes; SdC, Sierra de los Colorados; SRT, Sierra Santa Rosa de Tastil; n is the number of individual tracks measured or individual crystals dated; SD is the standard deviation of the mean track length.

these orographic barriers, condensing Atlantic-derived moisture along their eastern flanks, accounts for the climatic changes in the Angastaco region [*Starck and Anzótegui*, 2001; *Coutand et al.*, 2006].

3. Fission Track Dating

3.1. Methodology

[11] The AFT dating method records the cooling of rock suites below temperatures of ~110°C [*Green et al.*, 1989a, 1989b]. The use of this method relies on the fact that fission tracks form at a constant rate and are subsequently shortened and may eventually disappear in response to elevated temperatures. As a result, the track length distribution is a sensitive monitor of a crystal's thermal history. Significant fission track annealing occurs in a temperature interval between ~60 and 110°C, the partial annealing zone (PAZ); at significantly higher temperatures, annealing is geologically instantaneous. Annealing strongly depends on the kinetic characteristics of the apatites, reflected in the etch pit diameter (Dpar) [*Donelick et al.*, 1999; *Ketcham et al.*, 1999]. Apatites with large etch pit diameters are regarded as having higher thermal stabilities and hence higher total annealing temperatures than apatites with smaller etch pits [*Ketcham et al.*, 1999]. Thermal modeling provides a quantitative evaluation of the annealing behavior of a specific sample [e.g., *Ketcham et al.*, 2000].

[12] AFT data from exhumed basement rocks can be subdivided into two general groups, depending on the maximum temperature the sample was exposed to just prior to exhumation, the cooling rate and the kinetic characteristics of the apatite [e.g., *Green et al.*, 1989a]. Samples that cooled rapidly from temperatures exceeding the total annealing temperature (T_A, ~110°C) [*Ketcham et al.*, 1999] have long mean track lengths (MTL) with low standard deviations, and the apparent AFT age dates the cooling event [e.g., *Gleadow et al.*, 1986]. On an age-elevation plot the fission track ages from a vertical profile will plot on a more or less straight line, illustrating the rapid cooling history of the rocks [e.g., *Fitzgerald et al.*, 1995]. The slope of this line is the apparent exhumation rate. Reduced MTLs combined with higher standard deviations can be attributed to slow continuous cooling or to a reheating event due to reburial, where the maximum temperature the sample experienced was insufficient to reset the AFT clock. For moderately annealed samples (MTL > ~10 μm), the age reduction is proportional to the track length reduction [*Green*, 1988]; accordingly, corrected ages may yield rough estimates of the time the sample cooled below T_A, but are often inadequate for samples with more complex thermal histories.

[13] For age determinations, ~20 good quality grains per sample were selected at random and dated. For apatite track length analysis, 100 horizontal confined tracks and the angle between each track and the crystal's c axis were measured in each sample, provided 100 were present. To characterize the annealing properties of the apatites [*Donelick et al.*, 1999, *Ketcham et al.*, 1999], four Dpar measurements were averaged from each analyzed crystal. Following convention, all statistical uncertainties on ages and MTLs are quoted at the $\pm 1\sigma$ level, but $\pm 2\sigma$ uncertainties are taken into account for geological interpretations.

3.2. Analytical Results

[14] The mainly granitoid samples were collected along vertical profiles that extend from the base to the crest of the mountain range, spanning as much vertical distance as possible. All 21 samples analyzed in this study are monocompositional, as indicated by the low standard deviations of the Dpar values (0.05–0.10 μm), but considerable differences between samples occur (Table 1).

[15] The two dated samples from Sierra de Macon (MAC) (Figure 1a), with 370 m vertical distance between them, are characterized by early Jurassic ages (189 ± 11 and 198 ± 12 Myr), significantly shortened MTLs (11.6 ± 0.2 and 11.9 ± 0.2 μm), and similar Dpar values of about 2.24 μm (Table 1 and Figures 3 and 4). Simple corrections for track length reductions yield Middle Triassic ages (236 and 242 Myr).

[16] Eleven analyzed samples from Complejo Oire (CO) and Valle Luracatao (VL) from the western and eastern flank of the Cumbres de Luracatao, respectively (Figure 2), provide a 2450 m vertical profile. Plotting AFT age versus elevation (Figure 4), a straight line can be fit through all data points except samples CO7 and CO1, yielding an apparent exhumation rate of 0.5 mm/yr for the time interval between 20 ± 1 and 16 ± 1 Myr. Sample CO7 is not only notably older (56 ± 2 Myr) but also shows a shortened MTL of 12.4 ± 0.2 μm, suggesting that this sample is partially reset (Table 1 and Figure 3). In contrast, most other samples have longer MTLs between 12.8 and 14.2 μm and a limited age distribution between 16 ± 1 and 20 ± 1 Myr (Table 1 and Figures 3 and 4), indicating rapid cooling. Dpar values range between 1.99 and 2.25 μm, pointing to fairly similar chemical compositions (Table 1). Only two samples have slightly divergent ages. The higher Dpar (2.32 μm) of sample CO1 suggests a higher annealing resistance. This, and/or the low apatite quality could account for its older age (26 ± 2 Myr). Sample VL13, the only sample failing the χ^2 test (likely due to poor apatite quality), yielded a central age of 13 ± 2 Myr from only nine countable grains, and hence has low precision. The overall pattern of the vertical profile suggests exposure of a Cenozoic PAZ in the upper part and that exhumation started before 20 Myr. The apparent exhumation rate of 0.5 mm/yr would lead to an unreasonably thick section of removed material if rapid exhumation had continued up to the present; the data suggest that the rate decreased after ~16 Myr.

[17] Only one sample from Nevado de Cachi (CA) (Figure 2) could be dated, due to the overall low quality of the apatites. As the pooled age of 15 ± 2 Myr is calculated from only nine countable grains and no lengths could be measured (Table 1 and Figures 3 and 4), the precision and hence the geological meaning of this sample are uncertain. The high Dpar value (2.30 μm) points to thermally resistant apatite.

[18] At the range 10 km south of the village Colome (COL) (Figure 2), two analyzed samples spanning a 400 m vertical distance show sharply contrasting AFT results. The

Table 1. Apatite Fission Track Analytical Data[a]

Sample	Latitude, South	Longitude, West	Altitude, m	N_{XL}	Rho-S, $\times 10^6$ cm^{-2}	NS	Rho-I, $\times 10^6$ cm^{-2}	NI	P(χ^2), %	Rho-D, $\times 10^6$ cm^{-2}	ND	Age ± σ, Ma	U, ppm	Length ± σ, μm	SD_L, μm	N_L	Dpar, μm	SD_D, μm
								Sierra de Macon										
MAC 4	24°35.754′	67°19.390′	4540	20	1.1840	645	1.332	726	70	1.1095	4422	189.4 ± 11.2	15.0	11.58 ± 0.23	2.33	100	2.22	0.09
MAC 1	24°35.830′	67°19.848′	4170	20	0.7575	627	0.8276	685	9	1.1293	4422	198.4 ± 12.0	9.2	11.87 ± 0.18	1.77	100	2.26	0.10
								Complejo Oire										
CO7	24°58.787′	66°36.751′	5170	20	1.5160	1878	5.441	6742	60	1.0438	4422	56.4 ± 2.0	65.2	12.43 ± 0.19	1.89	100	2.13	0.07
CO6	24°58.862′	66°37.101′	4890	20	0.5724	927	5.758	9324	26	1.0503	4422	20.3 ± 0.9	68.5	14.20 ± 0.15	1.08	50	2.01	0.06
CO4	24°59.054′	66°37.688′	4520	20	0.4137	609	4.577	6738	39	1.0635	4422	18.7 ± 0.9	53.8	13.91 ± 0.15	1.09	50	1.96	0.07
CO1	24°59.225′	66°40.355′	4140	20	0.3823	344	3.126	2813	5	1.0832	4422	25.8 ± 1.6	36.1	14.16 ± 0.17	1.71	98	2.32	0.08
CO8	25°00.560′	66°42.273′	3860	20	0.6013	877	6.368	9288	39	1.0372	4422	19.1 ± 0.8	76.7	14.07 ± 0.11	0.99	82	2.01	0.09
								Valle Luracatao										
VL 14	25°19.946′	66°30.617′	3985	12	0.2870	143	3.798	1892	100	1.2341	5073	18.2 ± 1.6	38.5	-	-	-	1.99	0.09
VL 13	25°19.516′	66°30.822′	3740	9	0.2176	84	4.036	1558	<5	1.2437	5073	*13.2 ± 2.1*	40.6	-	-	-	2.01	0.07
VL 12	25°19.208′	66°30.279′	3530	20	0.6597	892	9.902	13390	32	1.2532	5073	16.3 ± 0.7	98.8	13.85 ± 0.18	1.58	80	2.07	0.08
VL 10	25°18.919′	66°29.646′	3170	20	0.6500	813	10.050	12571	84	1.2723	5073	16.0 ± 0.7	98.7	13.53 ± 0.19	1.45	56	2.05	0.10
VL 8	25°18.705′	66°29.521′	2830	20	0.6573	942	10.310	14770	51	1.2914	5073	16.0 ± 0.7	99.8	12.82 ± 0.24	1.91	61	2.00	0.06
VL 4	25°14.952′	66°25.539′	2810	20	0.6841	765	11.140	12454	73	1.3009	5073	15.6 ± 0.7	107.0	13.12 ± 0.19	1.89	100	2.25	0.05
								Nevado de Cachi										
CA8*	25°01.253′	66°20.438′	3700	9	0.4613	84	6.821	1242	77	1.1375	4678	15.0 ± 1.7	75.0	-	-	-	2.30	0.07
								Colome										
COL5*	25°34.049′	66°25.103′	2900	20	5.0910	4457	7.078	6197	<5	1.1672	4678	*162.4 ± 5.5*	75.8	11.29 ± 0.21	2.13	100	2.34	0.06
COL2*	25°34.246′	66°25.413′	2500	20	0.4109	502	5.581	6818	65	1.1771	4678	16.9 ± 0.9	59.3	13.15 ± 0.18	1.82	100	1.92	0.07
								Cerro Durazno										
CD 53	25°40.133′	66°19.213′	3380	19	2.2777	1421	10.570	6598	<5	1.2246	5073	*51.9 ± 2.6*	107.9	10.91 ± 0.24	2.36	100	2.16	0.10
CD 95	25°39.558′	66°21.563′	3300	22	3.8270	3384	9.998	8841	<5	1.1769	5073	*86.1 ± 3.4*	106.2	11.46 ± 0.17	1.70	100	2.16	0.10
CD 92	25°39.666′	66°21.227′	3110	20	4.1940	2956	10.140	7150	<5	1.1864	5073	*95.2 ± 3.7*	106.9	11.08 ± 0.18	1.82	100	2.24	0.08
CD 90	25°39.418′	66°21.126′	2950	20	4.5990	3560	11.610	8985	30	1.1960	5073	91.7 ± 2.8	121.3	11.00 ± 0.25	2.49	100	2.21	0.08
CD 87	25°39.292′	66°20.971′	2800	20	3.5110	2940	11.960	10020	21	1.2055	5073	69.0 ± 2.4	124.1	11.31 ± 0.19	1.86	100	2.20	0.09

[a]Sample preparation followed the procedure outlined by *Sobel and Strecker* [2003]. Apatites were etched for 20 s at 21°C with 5.5 mol nitric acid. Samples were analyzed with a Leica DMRM microscope or a Zeiss Axioplan microscope (samples labeled with an asterisk), both are provided with a drawing tube located above a digitizing tablet and a Kinetek computer-controlled stage driven by the FTStage 3.11 program [*Dumitru*, 1993]. Analysis was performed with reflected and transmitted light at 1250X magnification under dry objectives. Grains were dated by external detector method with muscovite detectors [*Gleadow*, 1981] that were etched for 45 min at 21°C with 40% hydrofluoric acid after irradiation at the well-thermalized TRIGA reactor at Oregon State University. Ages were calculated using the program MacTrack. The pooled age is reported for all samples that passed the χ^2 test; for samples with P(χ^2) < 5% the central age (italic numbers) is used. Error is ±1σ, calculated using the zeta calibration technique [*Hurford and Green*, 1983] with $\zeta = 389.9 \pm 7.5$ for apatite and CN5 glass (for A. Deeken). Abbreviations are as follows: N_{XL} is the number of individual crystals dated, Rho-S and Rho-I are the spontaneous and induced track density (tracks/cm^2) measured, respectively. N_S and N_I are the number of spontaneous and induced tracks counted, respectively. P(χ^2) (%) is the χ^2 probability. Rho-D is the induced track density (tracks/cm^2) in the external detector adjacent to the CN5 dosimetry glass. ND is the number of tracks counted in determining Rho-D; U is the uranium content. SD_L and N_L are the standard deviation of the track lengths and the numbers of lengths measured, respectively. SD_D is the standard deviation of the Dpar values.

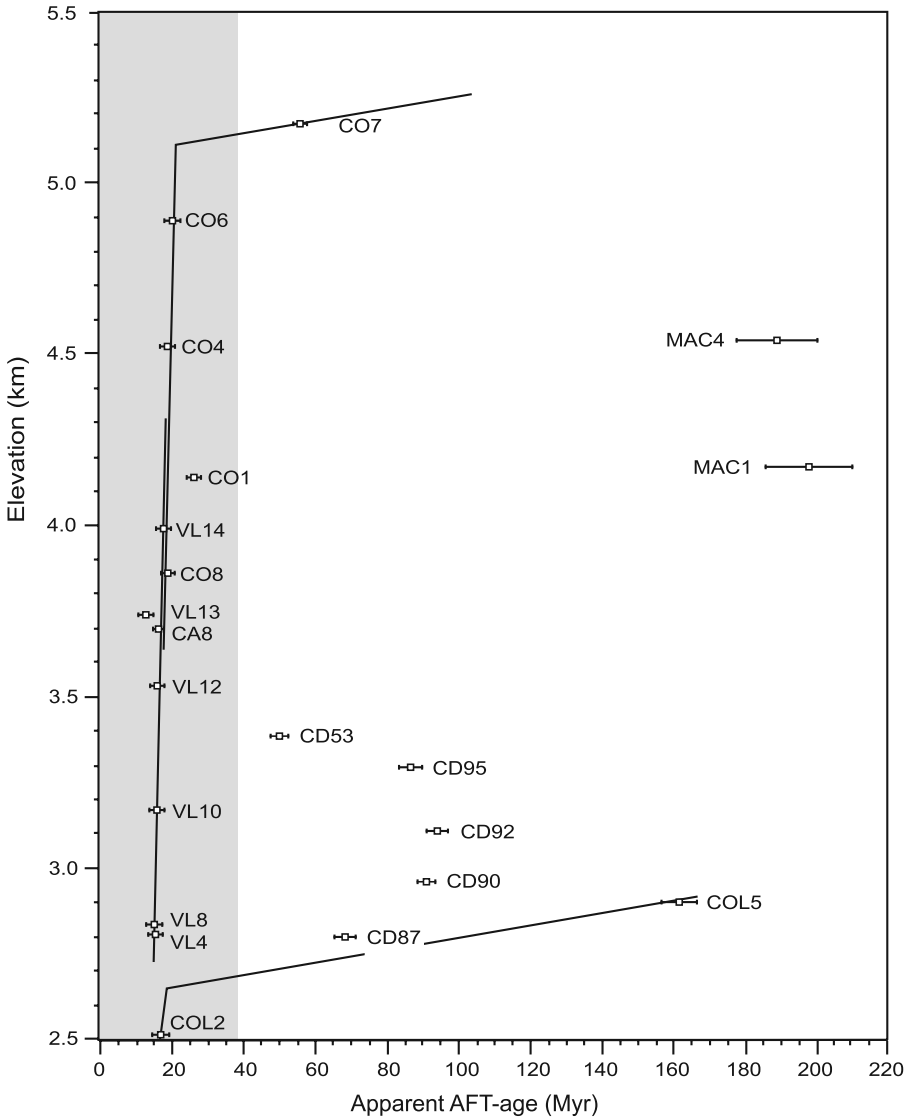

Figure 4. Summary of apparent AFT ages, plotted against sample elevation. The samples on the left side of the diagram (shaded area) are completely reset, whereas all samples on the right side are partially reset, suggesting that these samples resided in the PAZ for a longer time. The combination of partially and completely reset samples in two of the vertical profiles suggests that exhumation started before 20 Ma (CO/VL profile) and 19 Myr (COL profile). Error bars indicate 1σ error. For sample locations and abbreviations, see Figures 1a, 2, and 3.

topographically higher sample COL5 yields a central age of 162 ± 6 Myr and a high Dpar value of 2.34 μm (Table 1 and Figures 3 and 4); the significantly shortened MTL of 11.3 ± 0.2 μm due to a longer residence in the PAZ may account for the sample failing the χ^2 test. Correction for track length reduction yield a latest Triassic age (208 Ma). For sample COL2 a pooled age of 17 ± 1 Myr, a much lower Dpar value of 1.92 μm and a MTL of 13.2 ± 0.2 μm were measured (Table 1 and Figures 3 and 4), suggesting that it is completely reset.

[19] Four samples from a 500 m vertical transect at Cerro Durazno (CD) (Figure 2) yield apparent ages between 69 ± 2 and 95 ± 3 Myr; a sample collected from a range ~3 km to the east yields an age of 52 ± 3 Myr (Table 1 and Figures 3 and 4). The narrow Dpar distribution between 2.16 and 2.24 μm indicates monocompositional apatite. Significantly shortened MTLs between 10.9 ± 0.2 and 11.5 ± 0.2 μm are indicative of partial annealing that leads to mixed single grain ages; consequently, three of the samples fail the χ^2 test. Corrections for track length reductions yield exclusively middle Cretaceous ages (88 to 124 Myr). The lack of a systematic relationship between age and elevation (Figure 4) may be due to faults separating CD53 and CD95 from the three central samples; indeed,

Table 2. Description of the Incremental Modeling Approach[a]

	First Constraint		Second Constraint			3rd Constraint		
Sample	Time Range, Myr	T Range, °C	Time Range, Myr	Shifting Increments, Myr	T Range, °C	Time Range, Myr	Shifting Increments, Myr	T Range, °C
CO7	120	60–200	45–25	5	20–150	25–21	0.1	70–150
COL5	260	60–200	80–30	10	20–150	30–19	0.1	60–150 and 70–150
CD90, 92	180	60–200	49–20	1	20–150	30–4	1	20–150
CD53, 87, 95	140	60–200			20–150			
CO1, 4, 6, 8,	30–15[b]	60–200	-				-	
VL4, 8, 10, 12		60–200						
and COL2		60–200						

[a]Details about time and temperature ranges of the constraints used in the incremental modeling approach. All models were started at times approximately 1.5X greater than the apparent AFT age, with a temperature range between 60 and 200°C, such that all tracks initially formed could be completely annealed (first constraint). The final constraint was the present surface temperature of 20°C. For samples where the AFT data indicate rapid cooling (CO1, 4, 6, 8, VL4, 8, 10, 12 and COL2), 15 model runs with two constraints were performed, shifting the first constraint in 1 Myr increments from 30 to 15 Myr. To resolve the more complex thermal history of the remaining samples (CO7, COL5 and all CD samples), more model runs were required using two additional constraints. These allowed an early cooling (second constraint) followed by a late stage reheating event (third constraint), consistent with the Cenozoic depositional history. The temperature limits of the second constraint were loose (20–150°C), whereas for samples CO7 and COL5 the third constraint enforced minimum temperatures appropriate to the temperature of the topographically lower sample (CO6 and COL2, respectively). Final constraint is 20°C at 0 Myr for all models.

[b]Constraint shifted in 1 Myr increments.

there is an important Neogene reverse fault between CD53 and the remaining samples (Figure 2).

4. Thermal Modeling

4.1. Methodology

[20] Track length modeling helps resolve the thermal history of a sample. The AFTSolve program of *Ketcham et al.* [2000] is based on the annealing model of *Ketcham et al.* [1999]. This model includes the projection model of *Donelick et al.* [1999] that allows for track length anisotropy with respect to the crystallographic axis of the apatite. AFTSolve permits forward modeling using single grain ages, track lengths, the angle of the confined tracks to the c axis, and Dpar values. *Donelick et al.* [2005] encourage workers interested in using Dpar to conduct careful cross calibrations to compensate for subtle but inevitable variations in measurement equipment and procedures. Therefore our Dpar values were calibrated using a linear correction factor of 0.87, calculated by comparing Dpar measurements of two age standards (Durango and Fish Canyon Tuff) with those of *Ketcham et al.* [1999] [*Sobel and Seward*, 2006]. As annealing depends more on temperature than on time [*Green et al.*, 1989b], track length modeling can provide good constraints on both the T_A and the peak temperature a particular sample experienced during reheating. The time-temperature path (t,T path) prior to reheating as well as the timing and duration of reheating are less well constrained. However, totally reset samples from the same vertical profile can define the timing of final cooling.

[21] To convert t,T paths into spatial information either the prevailing paleogeothermal gradient or heat flow densities and thermal conductivities of the rock types must be known. Information on the present thermal state of the crust in the study area are scarce. Extrapolation from heat flow densities of about 80 mW/m^2, typical for the Bolivian Eastern Cordillera [*Springer and Förster*, 1998], suggests similar values for the region of the southern Eastern Cordillera. These values could be even higher due to Miocene volcanism and to thinned lithosphere beneath the Argentine Puna since the Pliocene [*Allmendinger et al.*, 1997; *Kay et al.*, 1994; *Whitman et al.*, 1996]. However, since changes in surface heat flow density develop over time [e.g., *Babeyko et al.*, 2002], heat flow values could also have been lower in the Miocene. From all thermal models of the CO/VL vertical profile, a paleogeothermal of 18 ± 8°C/km at 16/15 Myr was determined (see section 4.2). All of the sampled ranges consist of basement rocks that are likely to have relatively high thermal conductivities between 3.0 and 4.0 W/(mK) [*Blackwell and Steele*, 1988]; therefore heat flow densities between 50 and 80 mW/m^2 seem to be reasonable values for the entire cooling interval. For most sample locations it is likely that the basement rocks were reburied by Cenozoic sediments with much lower thermal conductivities. A reasonable candidate for the sedimentary cover is the base of the Payogastilla Group, composed mainly of coarse- to fine-grained sandstones and siltstones [*Díaz et al.*, 1987]. Therefore the thicknesses of the overlying strata will be calculated with a thermal conductivity of 2.0 W/(mK), assumed for a sandstone bulk composition [*Blackwell and Steele*, 1988], and for heat flow densities of 80 and 50 mW/m^2. Bedrock thicknesses will be based on the calculated 18°C/km geothermal gradient.

[22] For samples that yielded robust AFT data, thermal histories were modeled with c axis projected length and corrected Dpar values. Using the Monte Carlo random search, each model run had 10000 iterations with monotonic path segments and four half segments between adjacent constraints. Heating and cooling rates were not constrained. For details about the incremental modeling approach, see Table 2.

Table 3. Summary of Thermal Models for the CO/VL Profile and of Sample COL2[a]

Sample	Oldest Track, Myr	T_A, °C	T at Inflection Point, °C	Number of Models Analyzed
CO7	92–72	98–118	48–62	76
CO6	22.2–20.7	119–129	42–66	8
CO4	21.6–20.0	120–132	48–98	10
CO1	27.3–26.3	130–147	25–59	4
CO8[b]				
VL12[c]				
VL10	19.0–17.5	115–125	61–114	11
VL8	21.0–19.1	103–126	72–108	11
VL4	20.6–17.9	120–138	87–120	11
COL2	23.0–19.0	103–128	-	10

[a]For the temperature ranges at the inflection point (15/16 Myr), the minimum and maximum good fit boundaries are quoted; the total annealing temperature (T_A) is indicated by the temperature of the best fit at the oldest track of each model.
[b]No acceptable fits.
[c]No good fits.

[23] AFTSolve offers a range of solutions which are consistent with the observed data. For every model run the program determines the best fit as well as the boundaries of the good fit and the acceptable fit solutions. Good fit solutions are supported by the data, acceptable fit solutions can not be excluded by the data [*Ketcham et al.*, 2000]. The quoted time ranges of cooling and reheating intervals summarize the good fit boundaries of all selected models for each sample (Tables 3 and 4). These time frames will be broad for partially annealed samples, so the quoted intervals may apparently overlap. Modeling results including details about the oldest tracks and T_As are summarized in Tables 3 and 4.

[24] Perturbations of isotherms due to topography [e.g., *Safran*, 2003] were considered to have had no significant influence on the cooling paths of the samples, because there was almost no relief when late exhumation started disrupting the Oligocene sedimentary basin, and only ~2 km of rapid exhumation occurred, during which time the AFT ages were set. Advection of the isotherms as a consequence of thrusting [e.g., *Brown and Summerfield*, 1997; *Mancktelow and Grasemann*, 1997] was not taken into account, since transient models of the thermal structure of the crust would introduce more complexity than is warranted by the modeled data.

4.2. Modeling Results

[25] Modeling could not constrain the thermal history of the two Sierra de Macon samples, due to the lack of additional information about the geological context. Almost all combinations of constraints yielded good fit models (not shown); ages of the oldest modeled track range between 288 and 272 Myr for most of the models.

[26] Seven of the nine samples from Complejo Oire and Valle Luracatao with sufficient data for modeling yielded model runs with good fit results (VL4, 8 and 10, CO1, 4, 6 and 7; Tables 3 and 4 and Figure 5a); the diverging results of sample CO1 were not taken into account because of the poor apatite quality of this sample. All thermal models of the five structurally lower samples, performed with two constraints (Table 2), confirm the rapid cooling indicated by the AFT data (Figure 5a); ages of the oldest tracks increase toward the top of the profile (Table 3 and Figure 5a). Between 15 and 16 Myr all thermal models show a break in the t,T path, where cooling rates decrease (Figure 5a); the initial high cooling rate is also visible in the age-elevation plot (Figure 4). The drop in cooling rates is unlikely to be a modeling artefact, because all model runs had four half segments between adjacent constraints and hence the t,T paths were not fixed. In addition, inflections in the cooling path should occur at the same time for all samples, as no major faults dissecting the vertical profile were observed.

[27] The late stage cooling history of the partially annealed sample CO7 is defined by the t,T path of the topographically lower sample CO6. Assuming a paleogeothermal gradient of 18°C/km, the vertical distance of 280 m between sample CO6 and sample CO7 results in a temperature difference of ~5°C. At 22–21 Myr, the lower good fit boundary of sample CO6 is 108°C, hence sample CO7 should have experienced a minimum temperature of ~103°C at that time, and should have started to cool by

Table 4. Summary of Thermal Models of Partially Annealed Samples[a]

	Sample						
	CO7	COL5	CD95	CD92	CD90	CD87	CD53
Oldest track, Myr	92–72	260–238	130–116	179–145	173–136	103–93	93–87
T_A, °C	98–118	97–130	103–127	94–123	94–118	100–125	109–120
Resides at high temperatures until, Myr	55–40	150–90	118–110	120–85	120–80	-	-
First cooling until, Myr	35–22	80–40	95–50	60–40	65–48	85–50	80–50
Start of reheating, Myr	30–22	70–30	50–25	50–30	50–28	50–25	50–30
Peak of reheating, Myr	24–21	30–19	29–8	30–3	20–5	25–4	28–7
Peak reheating T, °C	70–85	69–95	73–100	73–101	74–102	82–99	87–113
Start of final cooling, Myr	22.5–21	25–19	19–3	12–3	12–4	12–3	20–7

[a]Thermal models of partially annealed samples suggest a reheating event caused by Andean foreland basin strata. The quoted time frames of cooling and reheating intervals summarize the good fit boundaries of all models for each sample; the possible time frames for partially annealed samples are broad, and therefore the quoted intervals may overlap. For the temperature ranges the minimum and maximum best fit values are quoted.

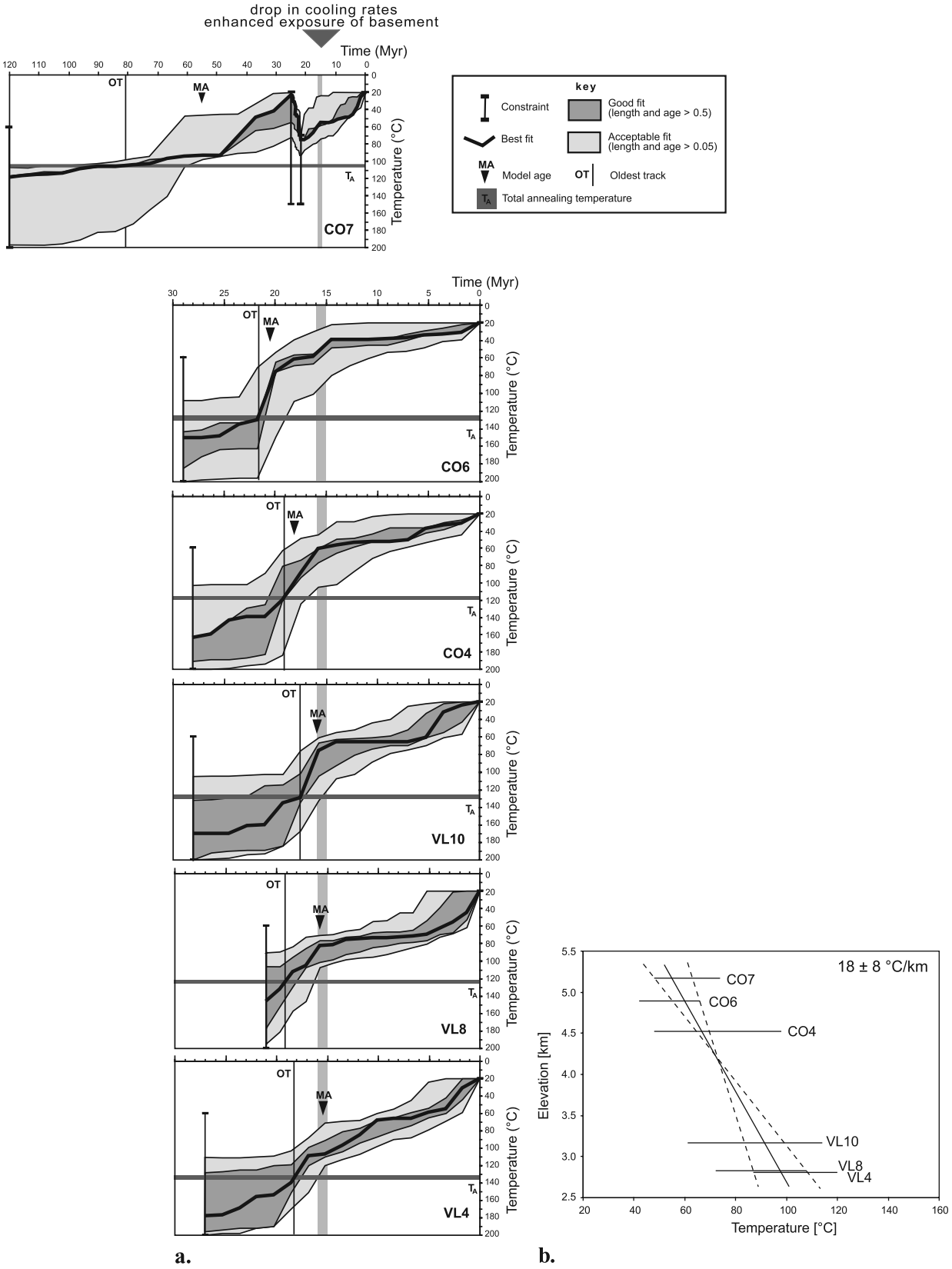
drop in cooling rates
enhanced exposure of basement
Time (Myr)
OT
MA
T_A
CO7
Temperature (°C)
key
Constraint
Best fit
Model age
Total annealing temperature
Good fit (length and age > 0.5)
Acceptable fit (length and age > 0.05)
Oldest track
CO6
CO4
VL10
VL8
VL4
a.
18 ± 8 °C/km
Elevation [km]
Temperature [°C]
b.

Figure 5

no later than 21 Myr. The shortened MTL of sample CO7 (Table 1 and Figure 3) requires slow cooling and/or a late stage reheating event. Models with two constraints allowing slow cooling yielded good fits only for temperatures $\leq$65°C at 22–21 Myr, which is in marked contrast to the expected results and precludes a simple cooling path of sample CO7. In order to better match the predicted temperatures, a series of models using four constraints were performed (Table 2). These allowed an early cooling (second constraint) followed by a late stage reheating event (third constraint), consistent with the Cenozoic depositional history discussed above. All three-stage cooling histories of sample CO7 are characterized by very slow cooling prior to 55–40 Myr, when rapid cooling commences (Figure 5a and Table 4). Initial cooling continues until 35–22 Myr, subsequent reheating starting at 30–22 Myr reaches peak temperatures of 70–85°C (best fit temperatures) between 24 and 21 Myr. At this time, the upper acceptable fit boundaries reach temperatures up to 104°C, and the ultimate cooling starts at 22.5–21 Myr, suggesting that samples CO6 and CO7 indeed share a common thermal history. However, a minor fault between the samples with ~550 m (~10°C) of vertical offset seems likely. Plotting the temperatures of the good fit boundaries of all six samples against sample elevation yields a paleogeothermal gradient of 18 ± 8°C/km at 16–15 Myr (Figure 5b).

[28] Since reheating is caused by reburial, the drop in cooling rates at 16–15 Myr may reasonably well be explained by a change in erodibility in the course of the exhumation history (see section 5.5). The peak reburial temperature of sample CO7 (70–85°C) (Table 4) results from an overlying rock column composed of Cenozoic sediments and basement rock; the respective portions can be estimated using the inflection point in the cooling path at 16–15 Myr (Figure 5a). The initial high cooling rate, likely caused by rapid removal of young, easily eroded sediments with low thermal conductivities, will decrease when more resistant bedrock with higher thermal conductivities is exposed [*Sobel and Strecker*, 2003, and references therein]. Therefore the difference between the peak reheating temperature (70–85°C) and the temperature at the inflection point (45–72°C) likely represents the removed sedimentary cover, whereas the difference between the temperature at the inflection point and the mean surface temperature (20°C) corresponds to the basement part. Analyzing individual best fit t,T path of 76 thermal models yields a thickness for the sediment column of 150–900 m and 200–1400 m for heat flow densities of 80 and 50 mW/m^2, respectively (Table 5). For a geothermal gradient of 18°C/km a thickness of the basement column of 1400–2600 m was calculated. Since 400 m of basement are preserved between sample CO7 and the crestal elevation, 1000–2200 m of basement have been completely removed by erosion. These estimates neglect unsteady heating behavior caused by rapidly deposited sediments [e.g., *Deming et al.*, 1990]. Such effects could reduce the amount of reheating and thereby increase the thickness of eroded sediments. Alternatively, advection of isotherms as a consequence of rapid erosional exhumation would lead to a decrease in the calculated thickness of eroded basement. In summary, estimates for the thickness of the total removed section range between 1600–2500 m and 2000–2800 m for the high and low heat flow density cases, respectively (Table 5). These values imply a mean denudation rate of 0.1 mm/yr for the entire cooling interval (Table 5).

[29] The sharply contrasting results of the two Colome samples could reflect differences in the kinetic behavior of the apatites, indicated by the different Dpar values, as well as displacement of the two samples by faults, although none were observed in the field. For sample COL2 the same modeling strategy as for the structurally lower CO/VL samples was used (Table 2). Rapid cooling started at 23–19 Myr (Figure 6a); at that time, the lower good fit boundary is 95°C. Assuming a common thermal history for the two samples, the minimum temperature sample COL5 experienced between 23 and 19 Myr should be ~90°C, due to the 400 m vertical distance between the two samples and a geothermal gradient of 18°C, and sample COL5 should have started to cool by no later than 19 Myr.

[30] The significantly shortened MTL of sample COL5 (Table 1 and Figure 3) suggests a reheating event caused by Cenozoic deposits. In addition, models with two constraints neglecting reheating did not yield good fit results. Therefore a series of thermal histories were modeled using a similar four-constraint approach as for sample CO7 (Table 2). Several models yielded appropriate good fit results with temperatures up to 95°C between 23 and 19 Myr (Figure 6b), corroborating the hypothesis that the thermally resistant apatites of sample COL5 are responsible for the discrepant apparent ages. In all of these models the sample resides at high temperatures until 150–90 Myr (Figure 6b and Table 4). Faster cooling (from 150 to 90 Myr on) lasts until 80–30 Myr in the different models. Beginning of reheating is possible between 70 and 30 Myr, reaching peak temperatures of 69–95°C between 30 and 19 Myr; final cooling commences between 25 and 19 Myr.

[31] Unlike the data for Cumbres de Luracatao, at Colome there is no data that allows us to differentiate between the portion of cooling due to removal of bedrock

Figure 5. (a) Representative AFTSolve models for the Complejo Oire and the Valle Luracatao samples. See Table 2 for modeling details. The top sample CO7 reveals a complex three-stage thermal history. Initial very slow cooling is superceded by enhanced cooling between 55 and 22 Myr. Subsequent reheating due to reburial by Andean foreland basin strata with peak temperatures of 70–87°C between 24 and 21 Myr reset the AFT ages of all structurally lower samples. Cooling of sample CO6 constrains the onset of Andean deformation-driven exhumation at 22.5–21 Myr. High cooling rates at the beginning of the ultimate exhumation can be attributed to rapid removal of overlying young sediments with low thermal conductivities. The decrease of cooling rates at 16–15 Myr (indicated by dark gray bars) is related to enhanced exposure of bedrock with higher thermal conductivities. (b) Modeled paleotemperatures of all CO and VL samples at 16/15 Myr, plotted against sample elevation, yielding a paleogeothermal gradient of 18 ± 8°C/km.

Table 5. Thicknesses of the Removed Rock Column, Calculated for Different Heat Flow Densities[a]

	Heat Flow Density, mW/m^2				
	Sediment Column, m		Mean Denudation Rate, mm/yr		
	80	50	80	50	Number of Models Analyzed
CO7	150–900	200–1400			76
CO7[b]	1600–2500	2000–2800	0.1		
COL5	1350–1900	2150–3000	0.1		97
CD95	1200–2400	1900–3800	0.2	0.4	94
CD92	1100–1850	1750–2950	0.2	0.3	87
CD90	1100–1700	1700–2750	0.2	0.3	78
CD87	1050–1650	1650–2650	0.2	0.4	82
CD53	1450–2150	2350–3450	0.2	0.3	74

[a]Thicknesses of the rock columns that were removed from the sample locations and erosion rates were calculated by analyzing individual best fit time-temperature paths of each sample. For rock columns the attained minimum and maximum values are quoted in 50-m bins, and mean values are quoted for denudation rates. To calculate basement thicknesses, a geothermal gradient of 18°C/km was assumed, for sediment thicknesses a thermal conductivity of 2.0 W/mK and heat flow densities of 80 and 50 mW/m^2 were used.
[b]Total eroded rock column.

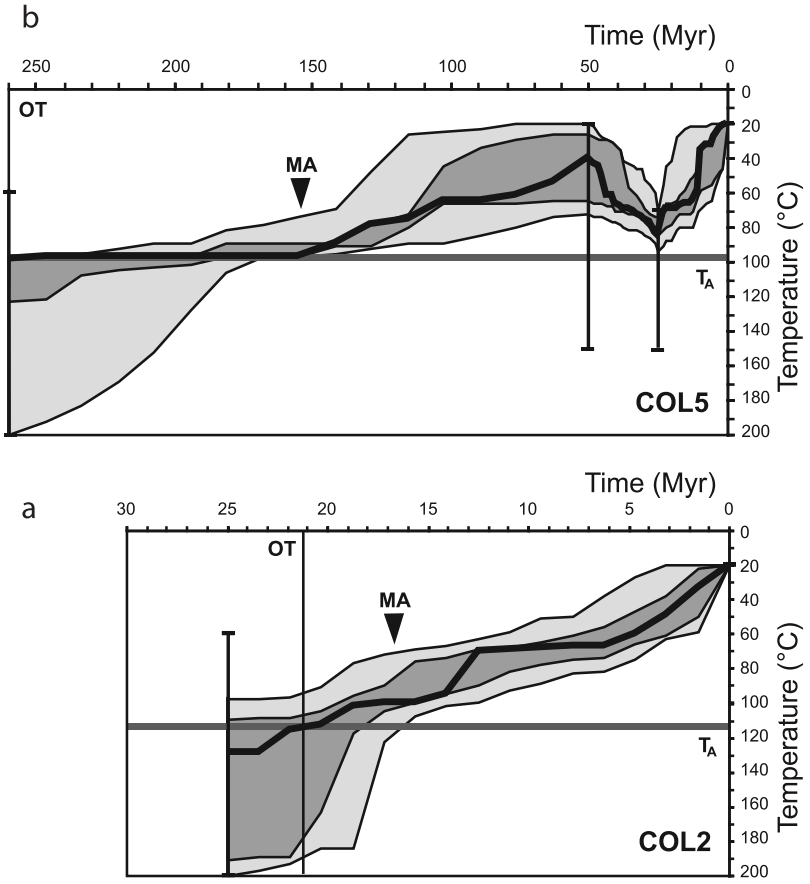

Figure 6. Representative AFTSolve models for the two Colome samples. For modeling details see Table 2; the key is the same as in Figure 5a. Note different age scales of the two models. (a) Exhumation during Andean deformation is defined by the completely reset sample COL2, and commenced between 23 and 19 Myr. (b) Initial cooling of sample COL5 is related to exhumation by normal faulting in Early Cretaceous time (Salta Rift), followed by reheating due to reburial beneath Andean foreland basin strata, peak reheating temperatures range between 70 and 90°C.

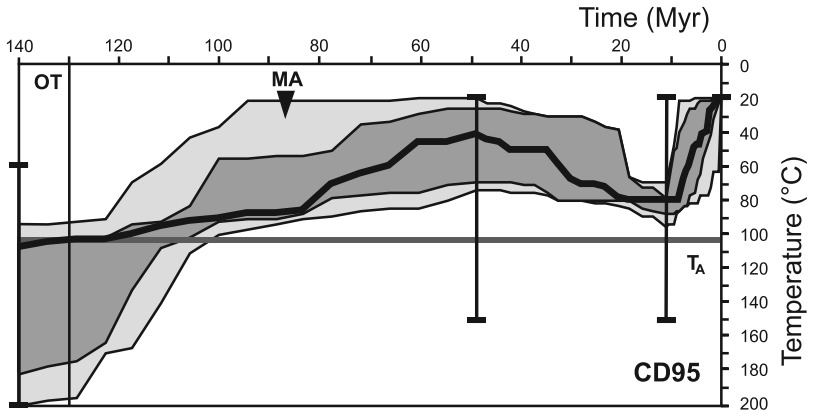

Figure 7. Representative AFTSolve model (CD95) for the Cerro Durazno samples. For modeling details, see Table 2; the key is the same as in Figure 5a. All of the Cerro Durazno samples have comparable thermal histories: The early, rift-related cooling history is similar to that of sample COL5;, reburial by Andean foreland basin strata commenced about in the same time interval (50–25 Myr), reaching similar peak temperatures (73–113°C), whereas the final cooling commenced definitively later (between 12 and 7 Myr) as at Cumbres de Luracatao and at Colome.

and sediment. Analyzing 97 individual best fit t,T paths suggests that, in the case where no basement was removed, a sediment column of 1350–1900 m and 2150–3000 m (for heat flow values of 80 and 50 mW/m^2, respectively) was eroded at a mean rate of 0.1 mm/yr (Table 5). The calculated proportion of sediment will decrease with increasing amount of basement, while the typical difference in thermal conductivities between these two lithologies implies that the total thickness of the rock column and, hence the erosion rate will increase.

[32] The relatively high Dpar value (2.30 μm) of the 15 Myr Nevado de Cachi sample suggest a high T_A; therefore a relatively thick section of overlying rock was required to reset the sample.

[33] All samples from Cerro Durazno are characterized by shortened MTLs (Table 1 and Figure 3), suggesting reburial by Cenozoic sediments. Models neglecting such a reheating event did not yield good fits. Unfortunately, no additional information about the time of final cooling from totally reset samples from the same vertical profile was available. A series of models with four constraints was performed with a broad range of possible time and temperatures frames (Table 2). Good fit model results were obtained from all five samples, all of them show comparable t,T paths (Figure 7 and Table 4). Early cooling from high temperatures commences between 130 and 80 Myr, and continues until 95–40 Myr in the different models. Beginning of reheating is possible between 50 and 25 Myr; peak reheating between 30 and 3 Myr reaches similar temperatures of 73–113°C for all samples. Final cooling may have started between 20 and 3 Myr; however, the most likely time is between 12 and 7 Myr, when the models of all samples overlap. In summary, the Cerro Durazno section shows Cretaceous cooling modified by reheating due to reburial beneath a Cenozoic sedimentary basin.

[34] As with sample COL5, the rock column that was removed from above Cerro Durazno was assumed to be composed merely of sediment, except for the basement remnants preserved above the samples, which yield a minimum amount for the basement thickness. Therefore the vertical distances between the samples and the crests of the range were converted into temperature, assuming a geothermal gradient of 18°C/km, and using a crestal elevation of 3.7 km for sample CD53 and of 3.5 km for the remaining samples. The resulting temperatures and the mean surface temperature were subtracted from the modeled peak reheating temperature (410 best fit t,T paths). The residual temperature implies that Cerro Durazno was formerly overlain by a 1050- to 2400-m-thick and 1650- to 3800-m-thick sediment column that experienced a mean denudation rate of 0.2 and 0.2–0.4 mm/yr (for heat flow values of 80 and 50 mW/m^2, respectively) (Table 5).

5. Discussion

[35] On the basis of our thermochronological data combined with geological information and published AFT data we propose a model for the tectonic development of the region of the present-day Puna and Eastern Cordillera at 25°S in four main steps (Figure 8): (1) Mesozoic-Paleocene extension, (2) Eocene-Oligocene deformation, (3) reburial by Andean foreland basin strata, and (4) Neogene exhumation during eastward propagating deformation.

5.1. Mesozoic-Paleocene Extension

[36] The old ages from Sierra de Macon may reflect an early, so far poorly known tectonic event in the region of the Salar de Arizaro basin in the Puna, possibly related to the Jurassic back-arc basin in Chile or even to a preceding Permo-Triassic transtensional rift stage [*Uliana and Biddle*, 1988]. The evolution of the Salta Rift is documented in the early thermal histories of the CD and COL5 samples (Figures 6, 7, and 8a). The onset of early cooling of the CD samples, between about 130 and 80 Myr, coincides with the early synrift phase in the Brealito subbasin [*Marquillas*

et al., 2005]. Horizontal extension during rifting was probably compensated by listric normal faulting and block tilting, leading to exhumation of the CD samples (Figure 8a). Postrift thermal relaxation may have contributed to continuous cooling, which is possible until 95–40 Myr. The range at Colome constituting the present eastern Puna margin was exhumed during approximately the same time interval from 150–90 Myr to 80–40 Myr (Table 4 and Figure 6b). This range was most likely part of the rift margin (Figure 1b), since synrift Pirgua deposits are only preserved on the basinward, eastern side of the range (Figure 2), and exhumation was accomplished by normal faulting along the main rift-bounding fault (Figure 8a). Consequently, the Cumbres de Luracatao were also part of the rift margin. The early very slow cooling of sample CO7 (from 90–76 Myr to 55–40 Myr) could be related to headward erosion of the rift shoulder and/or postrift thermal relaxation. Final filling of the rift basin during the postrift stage (Figure 8b), which was completed in the middle Eocene [*Mon and Salfity*, 1995], could have had some influence on the thermal histories of the Colome and Cerro Durazno samples, since reheating in the models is possible from 70 Myr and 50 Myr onward, respectively, although postrift strata are not preserved in the Brealito subbasin. This evolution of basement blocks formerly associated with rift shoulder exhumation of the Salta Rift is compatible with a similar Cretaceous history reflected in AFT data for the now exposed basement rocks of the Sierra de Quilmes and Cumbres Calchaquíes in the northern Sierras Pampeanas [*Sobel and Strecker*, 2003; *Mortimer et al.*, 2006].

5.2. Late Eocene-Oligocene Deformation

[37] In all thermal models of sample CO7, enhanced initial cooling commenced at about 55–40 Myr and lasted until ~35–22 Myr (Figure 5a). Although this cooling phase is manifest only in the thermal models of the least exhumed sample from the Complejo Oire, it likely reflects a major tectonic event in the eastern part of the present-day Andes, since it coincides with fast exhumation at other localities in the Argentine Eastern Cordillera [*Andriessen and Reutter*, 1994; *Coutand et al.*, 2001] and beginning of exhumation by 40–36 Myr in the central Eastern Cordillera of southern Bolivia [*Ege et al.*, 2006]. A fission track grain age population of 40.2–20.6 Myr in detrital apatites from the adjacent Angastaco basin suggests a late Eocene/Oligocene deformation episode in the present southern Eastern Cordillera [*Coutand et al.*, 2006]. This interpretation is furthermore corroborated by the intense erosion of the upper Pirgua Subgroup in the Brealito subbasin [*Boso et al.*, 1984], and the geometry of the unconformity demarcating the Andean foreland basin strata in the Angastaco region [*Grier et al.*, 1991]. The angle of the unconformity decreases from 27° west of Angastaco to 2–3° in the Tonco valley to the east, suggesting that uplift of the southern Salta Rift basin not only predated deposition of the Payogastilla Group, but also that uplift, at least in the westernmost part of the Angastaco basin, was associated with deformation [*Grier et al.*, 1991]. Because horizontal crustal shortening in late Eocene-Oligocene time is documented for different places on the Puna plateau [*Kraemer et al.*, 1999; *Adelmann*, 2001; *Coutand et al.*, 2001; *Carrapa et al.*, 2005], it is probable that the tectonic event responsible for exhumation in the Eastern Cordillera is of similar nature. Hence early exhumation at Complejo Oire was likely driven by thrust-faulting and subsequent erosional unroofing in the hanging wall (Figure 8c). The relief resulting from this early shortening phase was probably moderate, since the topographic high was subsequently beveled and the area was later reburied beneath Andean foreland basin strata (Figure 8d).

5.3. Reburial by Andean Foreland Basin Strata

[38] At Sierra de Macon, a small amount of reburial by Cenozoic strata is possible, but reheating was insufficient to reset the AFT ages. Sedimentary reburial may have started between 70 and 30 Myr at Colome (Figure 6b and Table 4), and approximately in the same time interval, between 50 and 25 Myr, at Cerro Durazno (Figure 7 and Table 4). This burial was thus contemporaneous with late Eocene-Oligocene deformation documented in neighboring regions. Early sedimentary deposits above Colome and Cerro Durazno were probably sourced from Complejo Oire and adjacent domains, erosionally exhumed at that time (Figure 8c). Reburial commenced somewhat later at Complejo Oire (30–22 Myr) (Figure 5a and Table 4); this area was the first to be exhumed in the final deformation phase (Figure 8e) (see section 5.4). Consequently, the duration and magnitude of reburial differ between the three sample locations: the thickness of the sedimentary cover calculated for sample COL5 (1350–3000 m) and the CD samples (1050–3800 m) is much higher than that calculated for sample CO7 (150–1400 m) (Table 5), although the uncertainties concerning the magnitude of basement eroded from Colome and Cerro Durazno preclude a precise comparison. The magnitude and timing of sedimentary reburial above Complejo Oire roughly correlate with the thickness (340–600 m) and the proposed Oligocene age [*Starck and Vergani*, 1996] of the Quebrada de los Colorados Formation that is preserved in the nearby Luracatao and Hualfin/Pucará valleys and in the Angastaco basin to the east (Figure 2). The strata of this formation pinch out to the east [*Starck and Anzótegui*, 2001] and were interpreted as foreland basin deposits associated with the late Eocene arc [*Russo and Serraiotto*, 1978; *Díaz and Malizzia*, 1983] or as the distal part of eastward prograding alluvial fans related to the Eocene-Oligocene Incaic orogenic phase [*Starck and Anzótegui*, 2001]. In an alternate scenario, deposition of this formation could be related to an Oligocene foreland basin that may have covered the basement rocks of all three ranges (Figure 8d). The coarser, basal part of this formation could also be associated with Eocene-Oligocene deformation. The basal strata of the overlying Angastaco Formation, exposed in the Hualfín and Pucará valleys (Figure 2), may have contributed to the sedimentary cover that had once buried Cerro Durazno (Figure 8f). However, better age constraints on the Quebrada de los Colorados Formation combined with provenance data are needed to further support this interpretation. Comparable peak reheating temperatures (69–113°C) of all partially reset samples (Table 4) suggest that these rocks resided at approx-

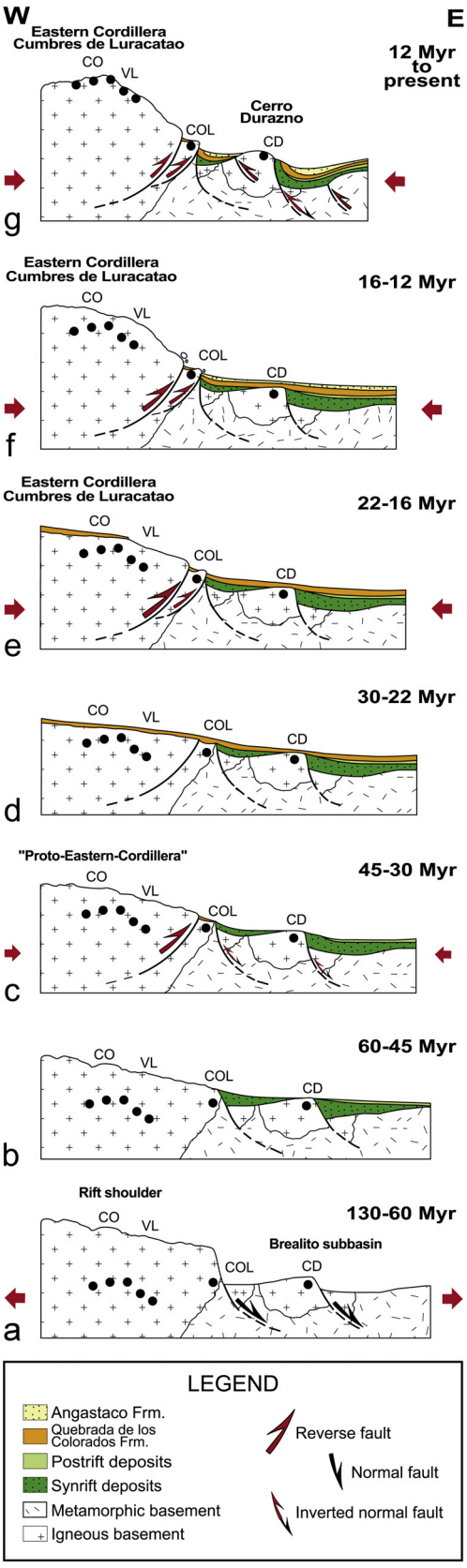

imately the same depth range within the Cenozoic PAZ (Figure 8d).

5.4. Pattern of Neogene Exhumation

[39] The data from Sierra de Macon, situated within the Puna plateau, point to a long period of protracted thermal stability with minimal exhumation and tectonic activity since the Jurassic, whereas the samples from the southern Eastern Cordillera document a phase of rapid cooling in the Miocene (Figures 5–7 and 8e–8g). The final cooling of the samples from Cumbres de Luracatao dates the onset of Andean deformation at the southern Eastern Cordillera between 22.5 and 21 Myr (Table 5), thereby defining the termination of deposition of the Quebrada de los Colorados Formation (Figure 8e). The ranges in the southern Eastern Cordillera formed by displacement on reverse and thrust faults [e.g., *Mon and Salfity*, 1995; *Marrett and Strecker*, 2000; *Riller and Oncken*, 2003]. At Cumbres de Luracatao this resulted in subsequent hanging wall erosion and hence cooling of the CO and VL samples. Comparable ages suggest that exhumation and hence deformation commenced about the same time at Colome (23–19 Myr) and at Nevado de Cachi (Tables 1 and 3). Exhumational unroofing of these samples continued, while the CD samples in the basin to the east were continuously heated by sedimentary reburial (Figures 8e and 8f). Only a broad time frame could be determined for the onset of final exhumation at Cerro Durazno, occurring most likely between 12 and 7 Myr (Figure 8g), and thus ~10–15 Myr later than at Cumbres de Luracatao. This timing is corroborated in the detrital record preserved in the adjacent Angastaco basin by a concomitant increased contribution of both low-grade metamorphic constituents and detrital apatites, sourced from Cerro Durazno [*Coutand et al.*, 2006]. Similarly, in a petrographic and magnetostratigraphic study of the Payogastilla Group *Butz et al.* [1995] reported an increase of sedimentary and metamorphic lithics at about 9.4 Myr. In agreement with observations at Sierra Aconquija [*Sobel and Strecker*, 2003], Sierra de Quilmes [*Kleinert and Strecker*, 2001], Cumbres Calchaquíes [*Strecker et al.*, 1989; *Bossi et al.*, 2001] and in the Angastaco Basin [*Díaz and Malizzia*, 1983; *Coutand et al.*, 2006], we propose that Neogene exhumation in this part of the southern central Andes

Figure 8. Schematic model for the development of the Cachi area, from rifting in the early Cretaceous and the subsequent development from a late rift and foreland basin setting to late Cenozoic construction of the southern Eastern Cordillera. Note that sample locations were projected onto a schematic E-W oriented structural profile. The black dots indicate sample positions. Not to scale. For sample locations and abbreviations see Figures 1, 2, and 3. (a) Synrift stage. (b) Postrift stage. (c) Late Eocene–Oligocene horizontal shortening. (d) Reburial by Andean foreland basin strata. (e) Onset of final exhumation at Cumbres de Luracatao. (f) Creation of significant topography at Cumbres de Luracatao. (g) Deformation propagates eastward, exhumation at Cerro Durazno.

propagated eastward, from Cumbres de Luracatao (between 22.5 and 21 Myr) and Colome (23–19 Myr) to Cerro Durazno (about 12–7 Myr) (Figures 1a and 2). Increasing magnitudes of burial from west to east suggest that, as the deformation front migrated, the basin depocenter also shifted eastward. Preliminary data from the Cobres Granite, a range north of Cumbres de Luracatao (Figure 1a) that was exhumed by no later than 25 Myr [*Deeken et al.*, 2005] suggest that deformation may also have propagated from north to south.

[40] The magnitude of Miocene exhumation is similar for all partially reset samples, since the calculated total removed section is approximately the same for the three sample locations: 1600–2800 m for Complejo Oire, 1350–3000 m for Colome, and between 1050 and 3800 m for Cerro Durazno (Table 5). In contrast, calculated mean erosion rates differ between Cerro Durazno (0.2–0.4 mm/yr), and Complejo Oire and Colome (0.1 mm/yr) (Table 5). These disparities may be related to increased humidity between 9 and 5 Myr in the Angastaco area and in the Santa María Basin to the south, documented by a significant change in paleoenvironment from arid to humid conditions [e.g., *Kleinert and Strecker*, 2001; *Starck and Anzótegui*, 2001; *Alonso et al.*, 2006]. The inferred period of more humid conditions lasted for a larger proportion of the cooling phase at Cerro Durazno (33–57%) compared to Complejo Oire and Colome (17–19%). In addition, the effect of increased precipitation on erosion rates was apparently stronger at Cerro Durazno, where it coincided with the removal of poorly consolidated and readily erodible sediments in the initial exhumation phase, whereas more resistant crystalline basement was then being exhumed at Complejo Oire and Colome.

5.5. Late Cenozoic Landscape Evolution

[41] Combining the exhumation history of the Eastern Cordillera with sedimentologic, stratigraphic and provenance data from the surrounding region provides information on landscape development. In the initial stage of tectonically driven rock uplift at Cumbres de Luracatao, variations in erosion rate were mainly controlled by rock resistance, fault geometry and shortening rate, since climate remained arid prior to deposition of the basal Palo Pintado Formation at about 9 Myr [*Starck and Anzótegui*, 2001; *Coutand et al.*, 2006]. In the early deformation phase, young sedimentary rocks could readily be removed (Figure 8e). Consequently, both exhumation and rock uplift rates were high, whereas the surface uplift rate likely remained relatively low (Figure 8e). As increasing amounts of resistant basement are exposed, exhumation rates decrease while surface uplift rates are expected to increase, if horizontal shortening rates remain steady [cf. *Burbank et al.*, 1999; *Sobel and Strecker*, 2003]. Potential effects of a gradual decrease in convergence rate between the Nazca and South America plates from about 20 Myr onward [*Somoza*, 1998] on tectonic activity in this region are difficult to assess, since the locus of deformation may shift even for constant relative plate motions.

[42] The Cumbres de Luracatao are oriented normal to moisture bearing, easterly winds [*Haselton et al.*, 2002]. Surface uplift of the range aided further aridifying the Puna basins to the west, where vast quantities of non-marine evaporites were deposited by no later than 14 Myr; these deposits have been interpreted as reflecting the formation of an orographic barrier [*Vandervoort et al.*, 1995]. In analogy with present conditions in NW Argentina, the range crest must have been at least 2000 m by that time [e.g., *Sobel and Strecker*, 2003]. The north-south trending growing barrier must have defeated the former eastward draining channel network, and thus prevented influx of the widespread volcanic material from the Puna. Indeed, volcanic constituents are limited in the sedimentary record of the Angastaco basin to the east [*Butz et al.*, 1995; *Coutand et al.*, 2006], suggesting that a drainage divide already existed at ~14.5 Myr, when the basal Angastaco Formation was deposited [*Coutand et al.*, 2006]. Conglomerate clasts from granitoid and metamorphic basement rocks at the base of this formation [*Coutand et al.*, 2006] could not have been deposited before faulting exposed resistant basement in the source region. Both sedimentary petrography and detrital AFT data suggest that a significant component of the Angastaco Formation was derived from the Cumbres de Luracatao [*Coutand et al.*, 2006]. Deposition of basement-derived conglomerates in the Angastaco basin corresponds to the decrease in cooling rates, implying that basement was already exposed at that time. The time when the orographic barrier was already established agrees well with the time when exhumation rates decrease (16–15 Myr) and the inferred accelerated range surface uplift. Thus the observed decrease in cooling rates, intensified by the difference in thermal conductivities of the two rock types, reasonably well demarcates the generation of significant topography from 16–15 Myr onward at Cumbres de Luracatao (Figure 8f).

[43] We infer a comparable history for Nevado de Cachi farther north. Both ranges, sloping away to the south and north from median summits, likely initiated as relatively small structures that were uplifted and gradually lengthened along strike with increasing amount of crustal shortening. Remnants of the basal Pirgua Subgroup, directly lying on basement and preserved at different elevations on the southern slope of the Nevado de Cachi [*Hongn and Seggiaro*, 2001], support the assumption of a lateral, southward directed growth of the ranges. In addition, both ranges may have coalesced with ranges to the north that were previously exhumed, as for example the Cobres Granite (Figure 1a) exhumed by no later than 25 Myr [*Deeken et al.*, 2005]. Similar to Cumbres de Luracatao, considerable surface uplift at Cerro Durazno probably postdated the initial phase of exhumation at 12–7 Myr, and the range followed a similar growth pattern. Pirgua strata are preserved at different elevations on the southern terminus of the range as well, and the Pucará syncline south of Cerro Durazno and Cerro Colorado (Figure 2) was most likely generated by southward propagating growth of the range. Uplift of these mountains divided the formerly continuous

basin into the Hualfín Basin to the west, and the Pucará and modern Angastaco Basins to the east. The eastern boundary of the Angastaco basin, the Sierra de los Colorados, was uplifted later in the Pliocene (Figure 3) [*Starck and Anzótegui*, 2001; *Coutand et al.*, 2006], emphasizing the eastward propagation of both deformation and range uplift.

[44] An open question concerns the link between the exhumation history of Cumbres de Luracatao and the depositional record in the Angastaco basin. One possibility is that for presently unknown structural reasons, the location of the basin was bypassed until 14.5 Ma. An alternative explanation involves the creation of accommodation space in the basin. Considerable quantities of sediments could not have accumulated before the throw along the range-bounding fault and the associated topographic load of the rising mountain range were great enough to create sufficient flexural accommodation space. In case of constant horizontal shortening rates, the time lag between the onset of deformation and creation of significant surface uplift depends primarily on the thickness of the overlying sediment column, as well as on climate, and hence on the erosion rate. The link between rock erodibility, rock uplift, and basin formation may thus explain the time lag of 6.5–8 Myr between the onset of cooling at Cumbres de Luracatao and the onset of sediment accumulation in the adjacent Angastaco basin. In accordance with observations made by *Sobel and Strecker* [2003] we suggest that such temporal lags may be characteristic in compressional tectonic settings where relatively fine-grained, poorly consolidated strata overlie resistant bedrock prior to the onset of range growth.

[45] To the extent that larger topographic loads require more work for a given increment of horizontal shortening and rock uplift, shortening as well as rock and surface uplift rates may diminish as topography grows and the locus of deformation shifts elsewhere in the range [e.g., *Masek and Duncan*, 1998; *Sobel et al.*, 2003]. If erosion in a given range is inefficient and its topography grows, the increased load may cause horizontal shortening rates to diminish, or deformation to shift entirely to a site requiring less work, as suggested by *Hilley et al.* [2005] for basement cored uplifts in the Sierras Pampeanas. In our case, deformation was forced to propagate into the foreland, thereby fragmenting the basin system into smaller compartments.

[46] The style of this propagating deformation is strongly influenced by inherited structures, in particular extensional structures of the former Salta Rift [*Bianucci et al.*, 1982; *Grier et al.*, 1991; *Cristallini et al.*, 1997; *Kley et al.*, 1999, 2005]. As a result of differential reactivation of these structures during Andean deformation and basin inversion, the base of synrift deposits is now exposed at different elevations on different fault blocks [*Hongn and Seggiaro*, 2001]. However, this could also be an effect of paleotopography. Samples CO7 and COL5, collected from elevations of 5170 and 2900 m, respectively, were initially situated at approximately the same depth in the Cenozoic PAZ beneath a surface of low relief (Figure 8d). The present vertical offset of 2270 m between the two sample localities suggests that considerable tectonic movement was focused along the reverse faults bounding the eastern flank of Cumbres de Luracatao (Figure 2); the displacement along these faults significantly contributes to local relief. This example shows that the depth of the partially reset samples (CO7, COL5 and all CDs) within the Cenozoic PAZ can be used as a structural marker for the displacement along the range-bounding reverse faults. Interestingly, the largest amount of rock uplift is accomplished along newly formed west dipping reverse faults that bound the eastern flank of the Cumbres de Luracatao, whereas inverted normal faults within the former rift basin accommodated only minor rock uplift (Figure 8g).

6. Conclusions

[47] Analysis of completely and partially reset AFT samples collected from vertical profiles on the Puna Plateau and across the southern Eastern Cordillera constrains the Cenozoic exhumation history in the southern central Andes. In addition, our data document the cooling history related to an earlier phase of rifting in the Cretaceous and an intervening episode of exhumation around 40–30 Myr that supports the inference of an early phase of horizontal crustal shortening and range uplift in the southern part of the Eastern Cordillera. These low-elevation ranges were subsequently eroded and partially buried beneath sediments that were part of a broad Andean foreland basin between 30 and 25 Myr. The oldest events in the geologic evolution of this area are revealed by thermal modeling of track length distributions, typically from structurally shallow samples. Thermal modeling also constrains the maximum reheating temperatures associated with reburial of the sample locations, and by inference, the thickness of the overlying rock columns. The duration of this episode of sedimentation and the calculated sediment thickness differ between the sample locations at the plateau margin, revealing an eastwardly propagating basin system. The onset of the ultimate phase of exhumation in the southern Eastern Cordillera is constrained by both age-elevation trends and modeling. Final exhumation commenced between 22.5 and 21 Myr at the present-day plateau margin and subsequently propagated eastward. Our AFT data document an earlier onset of late Cenozoic tectonic activity in this sector of the southern central Andes than previously thought. The eastward directed lateral growth of the Eastern Cordillera is coupled with a system of contractional basins that first advance in front of the range and then become subsequently compartmentalized by later emergent topography.

[48] Ranges in the study area which experienced significant Cenozoic exhumation also experienced Cretaceous exhumation associated with formation of normal faults in the Salta Rift. Structural studies suggest that Andean shortening often utilizes these older extensional structures. AFT data can show the position of samples within the PAZ prior to Andean deformation; this can be used as a proxy for the structural position and therefore helps constrain the relative displacement across different structures. At the southeastern plateau margin, reverse faults that were newly formed during Andean deformation are the dominant structures to accommodate horizontal crustal shortening.

[49] In summary, in the southern Eastern Cordillera, Cenozoic Andean deformation commenced by 22.5–21 Myr, earlier than previously suggested. The onset of deformation predates the inferred formation of significant topography there by 5–7.5 Myr and deposition of preserved strata in the adjacent Angastaco basin by 6.5–8 Myr. These lag times suggest that early, rapid exhumation is associated with removal of the sedimentary cover, while later, slower exhumation is linked with erosion of bedrock and more significant surface uplift; the latter is responsible for creating accommodation space in the adjacent flexural basin. Deformation and, by inference, range uplift in the study area thus propagated from west to east and from north to south.

[50] **Acknowledgments.** Assistance in the field and logistical support by Ruben Monaldi, Steffen Büttner, Ivan Petrinovic, and Fernando Hongn during collection of FT samples is greatly appreciated. Constructive reviews by Nadine McQuarrie and an anonymous reviewer significantly improved this paper; Ekkehard Scheuber provided helpful comments on an earlier version of the manuscript. This project is part of Collaborative Research Center (SFB) 267, "Deformationsprozesse in den Anden", funded by the German Research Foundation (DFG), and received additional financial support from the Freie Universität Berlin and Potsdam University, Germany. I. Coutand thanks the Alexander von Humboldt Foundation for providing funding during her stay at Potsdam University. We thank Onno Oncken for access to the Zeiss Axioplan microscope at the GFZ and S. Bonnet for providing the DEM of the southern central Andes in Figure 3. M. Strecker acknowledges additional support provided by D.F.G. and the A. Cox Fund of Stanford University.

References

Adelmann, D. (2001), Känozoische Beckenentwicklung in der südlichen Puna am Beispiel des Salar de Antofolla (NW-Argentinien), Ph.D. thesis, 180 pp., Freie Univ. Berlin, Berlin, Germany.

Allmendinger, R. W., and T. R. Zapata (1996), Imaging the Andean structure of the Eastern Cordillera on reprocessed YPF seismic reflection data, paper presented at XIIIth Congreso Geológico Argentino, Asoc. Geol. Argent., Buenos Aires, 13–18 Oct.

Allmendinger, R. W., V. A. Ramos, T. E. Jordan, M. Palma, and B. L. Isacks (1983), Paleogeography and Andean structural geometry, northwest Argentina, *Tectonics*, *2*, 1–16.

Allmendinger, R. W., T. E. Jordan, S. M. Kay, and B. L. Isacks (1997), The evolution of the Altiplano-Puna Plateau of the central Andes, *Annu. Rev. Earth Planet. Sci.*, *25*, 139–174.

Alonso, R. N. (1992), Estratigrafía del Cenozoico de la cuenca Pastos Grandes (Puna Salteña) con énfasis en la Formación Sijes y sus boratos, *Rev. Asoc. Geol. Argent.*, *47*, 189–199.

Alonso, R. N., J. Viramonte, and R. Y. Gutiérrez (1984), Puna Austral-Bases para el subprovincialismo geologico de la Puna Argentina, paper presented at Noveno Congreso Geológico Argentino, Asoc. Geol. Argent., San Carlos de Bariloche, Argentina, 5–9 Nov.

Alonso, R. N., T. E. Jordan, K. T. Tabutt, and D. S. Vandervoort (1991), Giant evaporite belts of the Neogene central Andes, *Geology*, *19*, 401–404.

Alonso, R. N., B. Carrapa, I. Coutand, M. Haschke, G. E. Hilley, E. R. Sobel, M. R. Strecker, and M. H. Trauth (2006), Tectonics, climate, and landscape evolution of the southern central Andes: The Argentine Puna Plateau and adjacent regions between 22 and 28°S lat, in *The Andes: Active Subduction Orogeny*, *Frontiers Earth Sci.*, edited by O. Oncken et al., pp. 265–283, Springer, New York.

Andriessen, P. A. M., and K.-J. Reutter (1994), K-Ar and fission-track mineral age determination of igneous rocks related to multiple magmatic arc systems along the 23° latitude of Chile and NW Argentina, in *Tectonics of the Southern Central Andes*, edited by K.-J. Reutter, E. Scheuber, and P. Wigger, pp. 141–153, Springer, New York.

Babeyko, A. Y., S. V. Sobolev, R. B. Trumbull, O. Oncken, and L. L. Lavier (2002), Numerical models of crustal scale convection and partial melting beneath the Altiplano-Puna plateau, *Earth Planet. Sci. Lett.*, *199*, 373–388.

Bianucci, H., J. F. Homovc, and O. M. Acevedo (1982), Inversión Tectónica y Plegamientos Resultantes en la Comarca Puesto Guardian-Dos Puntitas, Dep. Orán, Provincia de Salta, paper presented at 1. Congreso Nacional de Hidrocarburos, Inst. Argent. del Pet. Y del Gas, Buenos Aires.

Blackwell, D. D., and J. L. Steele (1988), Thermal conductivity of sedimentary rocks: Measurement and significance, in *Thermal History of Sedimentary Basins–Methods and Case Histories*, edited by N. D. Naeser and T. H. McCulloh, pp. 13–36, Springer, New York.

Blasco, G., E. O. Zappettini, and F. Hongn (1996), *Hoja Geológica San Antonio de los Cobres, 2566–I, Provincias de Jujuy y Salta, República Argentina, Bol. 217*, 126 pp., Subsecret. de Mineria de la Nacion, Dir. Nac. del Serv. Geol., Buenos Aires.

Boso, M. A., E. M. Brandán, and J. A. Salfity (1984), Estratigrafia y paleoambientes del Subgrupo pirgua (Cretácico) en la comarca de Brealito, provincia de Salta, paper presented at 9th Congreso Geológico Argentino, Asoc. Geol. Argent., La Plata, Argentina.

Bossi, G. E. (1969), Geología y estratigrafía del sector sur del valle de Choromoro, *Acta Geol. Lilloana*, *10*, 17–64.

Bossi, G. E., and M. Wampler (1969), Edad del Complejo Alto de las Salinas y Formación El Cadillal según el método K-Ar, *Acta Geol. Lilloana*, *10*, 141–160.

Bossi, G. E., S. M. Georgieff, I. J. C. Graviloff, L. M. Ibáñez, and C. M. Bruaga (2001), Cenozoic evolution of the intramontaine Santa María basin, Pampean Ranges, northwestern Argentina, *J. S. Am. Earth Sci.*, *14*, 725–734.

Brown, R. W., and M. A. Summerfield (1997), Some uncertainties in the derivation of rates of denudation from thermochronologic data, *Earth Surf. Processes Landforms*, *22*(3), 239–248.

Burbank, D. W., J. K. McLean, M. Bullen, K. Y.Abdrakhmatov, and M. M. Miller (1999), Partitioning of intermontane basins by thrust-related folding, Tien Shan, Kyrgyzstan, *Basin Res.*, *11*(1), 75–92.

Butz, D. J., C. P. Foldesi, and J. H. Reynolds (1995), Provenance of the Payogastilla Group: A preliminary uplift history of the central Andes, Salta Province, NW Argentina, *Geol. Soc. Am. Abstr. Programs*, *27*, 39.

Carrapa, B., D. Adelmann, G. E. Hilley, E. Mortimer, E. R. Sobel, and M. R. Strecker (2005), Oligocene uplift and development of plateau morphology in the southern central Andes, *Tectonics*, *24*, TC4011, doi:10.1029/2004TC001762.

Coutand, I., P. R. Cobbold, M. de Urreiztieta, P. Gautier, A. Chauvin, D. Gapais, E. A. Rossello, and O. López-Gamundí (2001), Style and history of Andean deformation, Puna plateau, northwestern Argentina, *Tectonics*, *20*, 210–234.

Coutand, I., B. Carrapa, A. Deeken, A. K. Schmitt, E. R. Sobel, and M. R. Strecker (2006), Orogenic plateau formation and lateral growth of compressional basins and ranges: Insights from sandstone petrography and detrital apatite fission-track thermochronology in the Angastaco basin, NW Argentina, *Basin Res.*, *18*, 1–26, doi:10.1111/j.1365-2117.2006.00283.x.

Cristallini, E., A. H. Cominguez, and V. A. Ramos (1997), Deep structure of the Metan-Guachipas region: Tectonic inversion in northwestern Argentina, *J. S. Am. Earth Sci.*, *10*(5–6), 403–421.

Deeken, A., E. R. Sobel, M. Haschke, and U. Riller (2005), Age of initiation and growth pattern of the Puna plateau, NW-Argentina, constrained by AFT thermochtonology, paper presented at 19th Colloquium on Latin American Geosciences, GeoForschungsZentrum Potsdam, Potsdam, Germany, 18–20 April.

Deming, D., J. A. Nunn, and D. G. Evans (1990), Thermal effects of compaction-driven groundwater flow from overthrust belts, *J. Geophys. Res.*, *95*, 6669–6683.

Díaz, J. I., and D. C. Malizzia (1983), Estudio geológico y sedimentológico del Terciario Superior del valle Calchaquí (departamento de San Carlos, provincia de Salta), *Bol. Sedimentol.*, *2*, 8–28.

Díaz, J. I., and A. Miserendino Fuentes (1988), El ambito deposicional y tectonico del Grupo Payogastilla (Provincia de Salta, Republica Argentina), paper presented at V Congreso Geológico Chileno, Soc. Geol. de Chile, Santiago, 8–12 Aug.

Díaz, J. I., D. C. Malizzia, and G. E. Bossi (1987), Análisis estratigráfico y sedimentológico del Grupo Payogastilla (Terciario superior), paper presented at X Congreso Geológico Argentino, Asoc. Geol. Argent., San Miguel de Tucumán, Argentina, 14–18 Sept.

Donelick, R. A., R. A. Ketcham, and W. D. Carlson (1999), Variability of apatite fission-track annealing kinetics: II. Crystallographic orientation effects, *Am. Mineral.*, *84*(9), 1224–1234.

Donelick, R. A., P. B. O'Sullivan, and R. A. Ketcham (2005), Apatite fission-track analysis, in *Low-Temperature Thermochronology: Techniques, Interpretations, and Applications*, *Rev. Mineral. Geochem.*, vol. 58, edited by P. W. Reiners and T. A. Ehlers, pp. 49–94, Mineral. Soc. of Am., Washington, D. C.

Dumitru, T. A. (1993), A new computer automated microscope stage system for fission track analysis, *Nucl. Tracks*, *21*, 575–580.

Ege, H., E. R. Sobel, E. Scheuber, and V. Jacobshagen (2006), Exhumation history of the southern Altiplano plateau (southern Bolivia), constrained by apatite fission track thermochronology, *Tectonics*, doi:10.1029/2005TC001869, in press.

Fitzgerald, P. G., R. B. Sorkhabi, T. F. Redfield, and E. Stump (1995), Uplift and denudation of the central Alaska Range: A case study in the use of apatite fission track thermochronology to determine absolute uplift parameters, *J. Geophys. Res.*, *100*, 20,175–20,191.

Galliski, M. A., and J. G. Viramonte (1988), The Cretaceous paleorift in northwestern Argentina: A petrological approach, *J. S. Am. Earth Sci.*, *1*(4), 329–342.

Gleadow, A. J. W. (1981), Fission-track dating methods: What are the real alternatives?, *Nucl. Tracks*, *5*, 3–14.

Gleadow, A. J. W., I. R. Duddy, P. F. Green, and J. F. Lovering (1986), Confined fission track lengths in apatite: A diagnostic tool for thermal history analysis, *Contrib. Mineral. Petrol.*, *94*, 405–415.

Green, P. F. (1988), The relationship between track shortening and fission track age reduction in apatite: Combined influences of inherent instability, annealing anisotropy, length bias and system calibration, *Earth Planet. Sci. Lett.*, *89*, 335–352.

Green, P. F., I. R. Duddy, A. J. W. Gleadow, and J. F. Lovering (1989a), Apatite fission-track analysis as a paleotemperature indicator for hydrocarbon exploration, in *Thermal History of Sedimentary Basins: Methods and Case Histories*, edited by N. D. Naeser and T. H. McCulloh, pp. 181–195, Springer, New York.

Green, P. F., I. R. Duddy, G. M. Laslett, K. A. Hegarty, A. J. W. Gleadow, and J. F. Lovering (1989b), Thermal annealing of fission tracks in apatite, 4. Quantitative modelling techniques and extension to geological timescales, *Chem. Geol.*, *79*, 155–182.

Grier, M. E. (1990), The influence of the Cretaceous Salta rift basin on the development of Andean structural geometries, NW Argentine Andes, Ph.D. thesis, Cornell Univ., Ithaca, New York.

Grier, M. E., and R. D. Dallmeyer (1990), Age of the Payogastilla Group: Implications for foreland basin development, NW Argentina, *J. S. Am. Earth Sci.*, *3*(4), 269–278.

Grier, M. E., J. A. Salfity, and R. W. Allmendinger (1991), Andean reactivation of the Cretaceous Salta rift, northwestern Argentina, *J. S. Am. Earth Sci.*, *4*(4), 351–372.

Haselton, K., G. Hilley, and M. R. Strecker (2002), Controls on mountain glaciation and paleoclimate implications: Evidence for stable climatic patterns in the southern Central Andes, *J. Geol.*, *110*, 211–226.

Hilley, G., and M. R. Strecker (2004), Processes of oscillatory basin filling and excavation in a tectonically active orogen: Quebrada del Toro Basin, NW Argentina, *Geol. Soc. Am. Bull.*, *117*, 887–901.

Hilley, G. E., P. M. Blisniuk, and M. R. Strecker (2005), Mechanics and erosion of basement-cored uplift provinces, *J. Geophys. Res.*, *110*, B12409, doi:10.1029/2005JB003704.

Hongn, F. D., and R. E. Seggiaro (2001), Hoja Geológica Cachi, 2566–III, Provincias de Salta y Catamarca, República Argentina, *Bol. 248*, 87 pp., Inst. de Geol. y Recursos minerales, Serv. Geol. Minero Argent., Buenos Aires.

Hurford, A. J., and P. F. Green (1983), The zeta age calibration of fission-track dating, *Chem. Geol.*, *41*, 285–317.

Jordan, T. E. (1984), Cuencas, vulcanismo y acortamientos cenozoicos, Argentina, Bolivia y Chile, 20–28°S latitud sur, paper presented at IX Congreso Geológico Argentino, Asoc. Geol. Argent., San Carlos de Bariloche, Argentina, 5–9 Nov.

Jordan, T. E., and R. N. Alonso (1987), Cenozoic stratigraphy and basin tectonics of the Andes Mountains, 20°–28° south latitude, *Am. Assoc. Pet. Geol. Bull.*, *71*(1), 49–64.

Jordan, T. E., J. H. Reynolds, and J. P. Erikson (1997), Variability in age of initial shortening and uplift in the central Andes, 16–33°30′S, in *Tectonic Uplift and Climate Change*, edited by W. F. Ruddiman, pp. 41–61, Springer, New York.

Kay, S. M., B. Coira, and J. Viramonte (1994), Young mafic back-arc volcanic rocks as indicators of continental lithospheric delamination beneath the Argentine Puna plateau, central Andes, *J. Geophys. Res.*, *99*, 24,323–24,339.

Ketcham, R. A., R. A. Donelick, and W. D. Carlson (1999), Variability of apatite fission-track annealing kinetics: III. Extrapolation to geological time scales, *Am. Mineral.*, *84*(9), 1235–1255.

Ketcham, R. A., R. A. Donelick, and M. B. Donelick (2000), AFTSolve: A program for multi-kinetic modeling of apatite fission-track data, *Geol. Mater. Res.*, *2*(1), 1–32.

Kley, J., C. R. Monaldi, and J. A. Salfiti (1999), Along-strike segmentation of the Andean foreland: Causes and consequences, *Tectonophysics*, *301*, 75–94.

Kley, J., E. A. Rossello, C. R. Monaldi, and B. Habighorst (2005), Seismic and field evidence for selective inversion of Cretaceous normal faults, Salta rift, northwest Argentina, *Tectonophysics*, *399*(1–4), 155–172.

Kleinert, K., and M. R. Strecker (2001), Changes in moisture regime and ecology in response to late Cenozoic orographic barriers: The Santa Maria Valley, Argentina, *Geol. Soc. Am. Bull.*, *113*, 728–742.

Kraemer, B., D. Adelmann, M. Alten, W. Schnurr, K. Erpenstein, E. Kiefer, P. van den Bogaard, and K. Görler (1999), Incorporation of the Paleogene foreland into the Neogene Puna plateau: The Salar de Antofalla area, NW Argentina, *J. S. Am. Earth Sci.*, *12*(2), 157–182.

Mancktelow, N. S., and B. Grasemann (1997), Time-dependent effects of heat advection and topography on cooling histories during erosion, *Tectonophysics*, *270*, 167–195.

Marquillas, R., and J. A. Salfity (1988), Tectonic framework and correlations of the Cretaceous-Eocene Salta Group, Argentina, in *The Southern Central Andes*, *Lect. Notes Earth Sci.*, vol. 17, edited by H. Bahlburg, C. Breitkreuz, and P. Giese, 119–136, Springer, New York.

Marquillas, R. A., C. del Papa, and I. F. Sabino (2005), Sedimentary aspects and paleoenvironmental evolution of a rift basin: Salta Group (Cretaceous-Paleogene), northwestern Argentina, *Geol. Rundsch.*, *94*, 94–113, doi:10.1007/s00531-004-0443-2.

Marrett, R., and M. R. Strecker (2000), Response of intracontinental deformation in the central Andes to late Cenozoic reorganization of South American Plate motions, *Tectonics*, *19*, 452–467.

Masek, J. G., and C. C. Duncan (1998), Minimum-work mountain building, *J. Geophys. Res.*, *103*, 907–917.

Mon, R., and J. A. Salfity (1995), Tectonic evolution of the Andes of northern Argentina, in *Petroleum Basins of South America*, edited by A. J. Tankard, R. Sàrez S., and H. J. Welsink, *AAPG Mem.*, *62*, 269–283.

Mortimer, E., B. Carrapa, I. Coutand, L. Schoenbohm, E. R. Sobel, J. Sosa Gomez, and M. R. Strecker (2006), Fragmentation of a foreland basin in response to out-of-sequence basement uplifts: El Cajon-Campo del Arenal basin, NW Argentina, *Geol. Soc. Am. Bull.*, in press.

Riller, U., and O. Oncken (2003), Growth of the central Andean Plateau by tectonic segmentation is controlled by the gradient in crustal shortening, *J. Geol.*, *111*, 367–384.

Riller, U., I. Petrinovic, J. Ramelow, M. Strecker, and O. Oncken (2001), Late Cenozoic tectonism, collapse caldera, and plateau formation in the central Andes, *Earth Planet. Sci. Lett.*, *188*, 299–311.

Russo, A., and A. Serraiotto (1978), Contribución al concocimiento de la estratigrafía Terciaria en el noroeste Argentino, paper presented at VII Congreso Geológico Argentino, Asoc. Geol. Argent., Neuquen, Argentina, 9–15 April.

Safran, E. B. (2003), Geomorphic interpretation of low-temperature thermochronologic data: Insights from two-dimensional thermal modeling, *J. Geophys. Res.*, *108*(B4), 2189, doi:10.1029/2002JB001870.

Salfity, J. A. (1980), Estratigrafía de la Formación Lecho (Cretácico) an la Cuence Andina del Norte Argentino, Ph.D. thesis, 91 pp., Univ. Nac. de Salta, Buenos Aires.

Salfity, J. A. (1982), Evolución paleogeográfica del grupo Salta (Cretácico-Eogénico), Argentina, paper presented at V Congreso Latinoamericano de Geología, Org. por el Serv. Geol. Nac., Subsecret. de Minería, Buenos Aires, 17–22 Oct.

Salfity, J. A., and R. A. Marquillas (1994), Tectonic and sedimentary evolution of the Cretaceous-Eocene Salta Group basin, Argentina, in *Cretaceous Tectonics of the Andes*, edited by J. A. Salfity, pp.266–315, Vieweg, Braunschweig, Germany.

Salfity, J. A., S. A. Gorustovich, M. C. Moya, and R. Amengual (1984), Marco tectónico de la sedimentación y efusividad Cenozoicas en la Puna Argentina, paper presented at IX Congreso Geológico Argentino, Asoc. Geol. Argent., San Carlos de Bariloche, Río Negro, Argentina, 5–9 Nov.

Sobel, E. R., and D. Seward (2006), Influence of etching conditions on apatite fission track etch pit diameter, in *European Conference on Thermochronology, Bremen, Germany, July 30–August 4*, *Schrift. Dtsch. Ges. Geowis.*, *49*, 128–130.

Sobel, E. R., and M. R. Strecker (2003), Uplift, exhumation and precipitation: Tectonic and climatic control of Late Cenozoic landscape evolution in the northern Sierras Pampeanas, Argentina, *Basin Res.*, *15*, doi:10.1046/j.1365-2117.2003.00214.x.

Sobel, E. R., G. E. Hilley, and M. R. Strecker (2003), Formation of internally drained contractional basins by aridity-limited bedrock incision, *J. Geophys. Res.*, *108*(B7), 2344, doi:10.1029/2002JB001883.

Somoza, R. (1998), Updated Nazca (Farallon)-South America relative motions during the last 40 Myr: Implications for mountain building in the central Andean region, *J. S. Am. Earth Sci.*, *11*, 211–215.

Springer, M., and A. Förster (1998), Heat-flow density across the central Andean subduction zone, *Tectonophysics*, *291*, 123–139.

Starck, D., and L. M. Anzótegui (2001), The late Miocene climatic change-persistence of a climatic signal through the orogenic stratigraphic record in northwestern Argentina, *J. S. Am. Earth Sci.*, *14*, 763–774.

Starck, D., and G. Vergani (1996), Desarollo Tecto-Sedimentario del Cenozoico en el Sur de la Provincia de Salta-Argentina, paper presented at XIII Congreso Geológico Argentino y tercero Congreso de Exploracíon de Hidrocarburos, Asoc. Geol. Argent., Buenos Aires, Argentina, 13–18 Oct.

Strecker, M. R., P. Cerveny, A. L. Bloom, and D. Malizia (1989), Late Cenozoic tectonism and landscape development in the foreland of the Andes: Northern Sierras Pampeanas (26°–28°S), *Tectonics*, *8*, 517–534.

Uliana, M. A., and R. T. Biddle (1988), Mesozoic-Cenozoic paleogeographic and geodynamic evolution of southern South America, *Rev. Brasil. Geoci.*, *18*, 172–190.

Vandervoort, D. S., T. E. Jordan, P. K. Zeitler, and R. N. Alonso (1995), Chronology of internal drainage development and uplift, southern Puna plateau, Argentine central Andes, *Geology*, *23*, 145–148.

Whitman, D., B. L. Isacks, and S. Mahlburg Kay (1996), Lithospheric structure and along-strike segmentation of the central Andean Plateau: Seismic Q, magmatism, flexure, topography and tectonics, *Tectonophysics*, *259*, 29–40.

I. Coutand, UMR-CNRS 8110, UFR des Sciences de la Terre (bât.SN5), Université des Sciences et Technologies de Lille 1, F-59655 Villeneuve d'Ascq cedex, France.

A. Deeken, Institut für Geowissenschaften, Freie Universität Berlin, Malteserstr. 74-100, D-12249 Berlin, Germany. (adeeken@zedat.fu-berlin.de)

M. Haschke, School of Earth, Ocean and Planetary Sciences, Cardiff University, Parc Place, Cardiff CF10 3YE, UK.

U. Riller, Museum, Humboldt Universität Berlin, Invalidenstr. 43, D-10115 Berlin, Germany.

E. R. Sobel and M. R. Strecker, Institut für Geowissenschaften, Universität Potsdam, Postfach 60 15 53, D-14415 Potsdam, Germany.